ARMY RESEARCH LABORATORY

ARL

Hot Explosive Consolidation
of W-Ti Alloys

Laszlo J. Kecskes
U.S. ARMY RESEARCH LABORATORY

Ian W. Hall
UNIVERSITY OF DELAWARE

ARL-TR-669

January 1995

DTIC
SELECTED
FEB 21 1995
B

19950207 003

NOTICES

REPORT DOCUMENTATION PAGE

Public reporting burden for this collection of information is estimated to average 1 hour per response, including the time for reviewing instructions, searching existing data sources, gathering and maintaining the data needed, and completing and reviewing the collection of information. Send comments regarding this burden estimate or any other aspect of this collection of information, including suggestions for reducing this burden, to Washington Headquarters Services, Directorate for Information Operations and Reports, 1215 Jefferson Davis Highway, Suite 1204, Arlington, VA 22202-4302, and to the Office of Management and Budget, Paperwork Reduction Project (0704-0188), Washington, DC 20503.

1. AGENCY USE ONLY (Leave blank)	2. REPORT DATE January 1995	3. REPORT TYPE AND DATES COVERED Final, Oct 91–Apr 93

4. TITLE AND SUBTITLE

Hot Explosive Consolidation of W-Ti Alloys

5. FUNDING NUMBERS

PR: 1L161102AH43
WU: 61102A

6. AUTHOR(S)

Laszlo J. Kecskes and Ian W. Hall*

7. PERFORMING ORGANIZATION NAME(S) AND ADDRESS(ES)

U.S. Army Research Laboratory
ATTN: AMSRL-WT-WD
Aberdeen Proving Ground, MD 21005-5066

8. PERFORMING ORGANIZATION REPORT NUMBER

9. SPONSORING/MONITORING AGENCY NAME(S) AND ADDRESS(ES)

U.S. Army Research Laboratory
ATTN: AMSRL-OP-AP-L
Aberdeen Proving Ground, MD 21005-5066

10. SPONSORING/MONITORING AGENCY REPORT NUMBER

ARL-TR-669

11. SUPPLEMENTARY NOTES

*Professor Ian W. Hall is the Chairman of the Materials Science Program at the University of Delaware.

12a. DISTRIBUTION/AVAILABILITY STATEMENT

Approved for public release; distribution is unlimited.

12b. DISTRIBUTION CODE

13. ABSTRACT (Maximum 200 words)

High density (98% T.D.) 95W-5Ti (wt.%) alloys have been fabricated by a hot explosive consolidation (HEC) technique. In the current procedure, a W+Ti powder compact is preheated by the heat released by a Ti+C exothermic combustion synthesis reaction and subsequently consolidated by pressure waves generated by the detonation of an explosive. The amount of explosive charge, sample configuration, and molar ratio of exothermic material to sample were found to affect the degree of consolidation. Auxiliary temperature measurements were performed to determine the precompaction thermal history of the sample to obtain the optimum delay time for consolidation. As observed with scanning electron microscopy, the HEC microcomposites consist of W particles surrounded by a partially discontinuous Ti-rich matrix. Transmission electron microscopy was also used to further characterize the W/Ti interfacial region. The pertinent features of the technique as well as those of the product microstructures are discussed.

14. SUBJECT TERMS

hot explosive compaction, dynamic consolidation, SHS, combustion synthesis, processing, microstructure, morphology, SEM, TEM, precursors, tungsten, tungsten alloy, titanium, titanium carbide

15. NUMBER OF PAGES
59

16. PRICE CODE

17. SECURITY CLASSIFICATION OF REPORT UNCLASSIFIED	18. SECURITY CLASSIFICATION OF THIS PAGE UNCLASSIFIED	19. SECURITY CLASSIFICATION OF ABSTRACT UNCLASSIFIED	20. LIMITATION OF ABSTRACT UL

INTENTIONALLY LEFT BLANK.

ACKNOWLEDGMENTS

iii

INTENTIONALLY LEFT BLANK.

TABLE OF CONTENTS

INTENTIONALLY LEFT BLANK.

LIST OF FIGURES

1. INTRODUCTION

In the ballistic community, the development of long-rod kinetic energy (KE) penetrators is an ongoing research effort. The two primary KE penetrator materials are those made from depleted uranium (DU) (T_m U = 1,240° C), and those made from tungsten (T_m W = 3,410° C) based heavy alloys (WHA) [1]. DU alloys, nominally U-0.75Ti (wt.%), are usually homogeneous, cast materials, which are subsequently worked and heat treated to obtain the desired mechanical properties. The strengthening mechanism in DU is attributed to a lenticular martensite microstructure [2,3]. In contrast, because of the refractory nature of W, WHA can only be produced by liquid-phase sintering (LPS). WHA are two-phase composites, essentially consisting of spheroidal tungsten particles embedded in a nickel-iron or copper-nickel matrix [4]. Recent scale model ballistic studies have demonstrated that a penetrator's performance does not depend on the mechanical and engineering properties of the material but rather on its ability to fail by the formation of adiabatic shear bands at oblique planes with respect to the penetrator-target interface [5].

Adiabatic shear bands are strain localization instabilities which develop when thermal softening exceeds work hardening. Adiabatic shear localization can occur at high-strain rates (i.e., the duration of the event is too short) or at low-thermal diffusivities (i.e., the temperature is low). During penetration, under the high rates of deformation (strain and strain-rate hardening), the heat generated in a narrow region of the material cannot be transported out, and a rapid rise in temperature results. Consequently, in materials that soften, due to rising temperatures, more rapidly than strengthen from hardening mechanisms, the material's load bearing capacity decreases [6,7]. This is an instability, since any changes in the strain field cause all subsequent deformation to localize in this weaker region [8].

Magness has demonstrated that the penetration of DU is by adiabatic shear localization, whereas, the penetration of WHA is by plastic deformation [5]. Because of the health hazards associated with the use of DU alloys (predominantly the toxicity of uranium fumes and oxides), current efforts are underway to develop a new WHA with a matrix phase susceptible to adiabatic

shear instabilities. The requirements for such alloys are high density, high strength, high hardness, modest to high ductility, and easy machinability. The metallurgy of the composition must be such that no weak intermetallic phases are formed. Several metals and alloys are prone to adiabatic shear failure. These include titanium, Ti-6Al-4V, zirconium, hafnium, and certain steel alloys (e.g., 4340) [9]. Undesirable intermetallic phases, such as WZr_2, WHf_2, and those between W and Fe, usually form if a critical temperature is exceeded (WZr_2: T_c = 2,210° C; WHf_2: T_c = 2,510° C; WFe_2: T_c = 1,060° C, W_2Fe_3 (W_6Fe_7): T_c = 1,640° C, WFe: T_c = 1,220° C) [10]. Since no intermetallic phase is known for the W-Ti system, this combination is under primary consideration [11].

Powder Metallurgy (P/M) fabrication techniques, especially those involving refractory metals, are often sought out when conventional forming routes, such as melting, casting, and forging approaches are not suitable. Additionally, P/M is more economical since the near net-shape products, with nearly finished dimensions, significantly reduce the need for machining. Lastly, due to recent developments in powder precursor preparation, there is a greater control of both grain size and improved component distribution that can result in a more homogeneous structure [12–14].

As stated previously, WHA are fabricated via persistent liquid-phase sintering. During the past decade, an extensive collection of articles have been published in the area of sintering and liquid-phase sintering [15–17]. To illustrate the key steps in the LPS of WHA, the process is briefly summarized. Initially, the Ni and Fe powders (or Cu and Ni), forming the matrix in the heavy alloy, are premixed in a 7:3 weight ratio. The precursor W and the premixed Ni-Fe blend are further dry mixed together in a weight ratio of 90:10, or 93:7. The typical purity of the precursors is 99.9+%, while the starting size of the precursors is approximately 1–5 μm. A green compact, pressed from the powder blend, is heated at elevated temperatures, in a controlled atmosphere, for an extended period of time. At these temperatures, the W partially dissolves in the liquified matrix and, upon cooling, reprecipitates out of solution onto the remaining tungsten grains to form a uniform grain structure. The molten matrix ensures complete densification by rapid rearrangement followed by solution-reprecipitation. For additional control of the properties

2

of the alloys, LPS is usually followed by annealing. A direct consequence of the LPS process is the loss of the initial tungsten morphology and structure that is replaced by nearly pure W, 20–60 µm, precipitates in a predominantly W-Ni-Fe alloy matrix. The composition of the saturated solution in the matrix has an approximate composition of 54Ni-23Fe-23W (wt.%). The effects of temperature, time, and atmosphere, the use of additives, modification of the matrix composition, and gravity induced segregation effects, all can have widely varying consequences on the efficiency of the process as well as the mechanical properties of the tungsten alloy [18–29]. Other factors that could greatly affect the microstructural characteristics of the alloys include the contiguity of tungsten grains, stress corrosion, and embrittlement caused by postconsolidation oxidation and the formation of undesirable intermetallics in the matrix [30–32].

An approach similar to LPS is desired for the fabrication of W-Ti heavy alloys; however, such commercial processes are now unavailable. In addition to the more conventional P/M techniques attempted at the U.S. Army Research, Development, and Engineering Center (ARDEC) (LPS via hot isostatic pressing [HIP]), GTE Sylvania (now OSRAM Sylvania) (LPS and solid-state sintering via HIP), and at Westinghouse (Dynapak coextrusion through a die), alternate fabrication methods are being explored as well [33]. One such route envisions the use of dynamic compaction techniques to consolidate and sinter the powdered precursors into fully dense products.

The novelty of dynamic compaction originated in the fact that not only can metal and ceramic powders be consolidated, but both equilibrium and nonequilibrium structures can result from the passage of the shock wave. A shock wave can be generated by the detonation of an explosive, impact of a projectile, or a flyer plate driven by either compressed gas or an explosive [34–36]. In the usual compaction geometries, the application of the shock wave can be in a planar or cylindrical configuration. As the shock wave propagates through, and densifies a powder bed, it produces bonding between the adjacent particles. The mechanism of compaction can be divided into three stages: transitional restacking, plastic deformation, and cold working with or without particle fragmentation or attrition [37–39]. The transitional restacking stage refers to the flow of particles past each other rearranging themselves as determined by the forces exerted on

them. This stage involves the greatest movement and therefore the largest increase in density. In the second stage, the limiting interparticle friction forces of stage one are exceeded, and the particles deform plastically to fill the voids in the powder. At the microscopic level, the friction-generated deformation and skin heating cause the outer oxide contaminated surface of the particles to be stripped away, thereby allowing the formation of interparticle bonds. It is such bonding that develops the loosely held powder into a coherent body. The various interparticle bond mechanisms are solid bridges, mechanical interlocking, interfacial forces, adhesive forces, and electrostatic forces [39]. The final stage of compaction is attributed to plastic work hardening. In cases when the compaction forces exceed the breaking stress within the powder body, fragmentation and fracture of the particles can result. It must be recognized that these stages are not necessarily sequential and in some powders, such as ceramic and brittle metal, the second stage is absent. In contrast, in extremely soft metals, like lead, stages one and three are of little significance.

Early studies of dynamic compaction of powdered tungsten concentrated on the measurements of porous (distended) solid Hugoniots (Pressure vs. Specific Volume dependence) and their prediction based on the Mie-Grueneisen equation of state [40–42]. Much of these works and others were aimed to identify the basic effects of shock stress amplitude, stress duration, as well as their correlation to microstructural and plastic deformation characteristics [43–45].

Due to the rapid densification rate, dynamically consolidated samples, including tungsten, often suffered from low nonuniform densities, poor interparticle bonding, and severe cracking [45]. High-detonation velocity explosives (6,000–8,000 m/s) tend to produce the desired hardness, interparticle bonding, and compressive strength, however, with profuse cracking. The cracking can be reduced or eliminated by using low-detonation velocity explosives (2,000–4,000 m/s), however, at the expense of consolidation quality.

Although there is a temperature rise due to the irreversible work during the consolidation of distended solids, in an attempt to avoid some of the former structural integrity problems, hot explosive consolidation (HEC) has been suggested [46,47]. In HEC, the precursor powder

4

mixture is placed in a sealed container, preheated in a high temperature furnace, quickly removed, transferred into the compaction fixture, and subsequently consolidated to full-density. The main advantages of preheating the powder are to decrease its yield strength, thereby increasing ductility, and to allow for greater thermal softening. Since Gorobtsov and Roman's article was published, HEC has been mentioned in several reviews and further explored by others [38,48–57]. A literature review of these latter works is provided in Appendix A.

At the U.S. Army Research Laboratory (ARL), Weapons Technology Directorate (WTD), a simpler variant of HEC is being applied to the consolidation of W-Ti alloys. In the WTD technique, referred to hereafter as Combustion Synthesis Assisted HEC (CSA-HEC), an in-situ TiC "chemical furnace" is used to preheat the powder sample prior to compaction [58]. The idea of chemical heating is not new and has been suggested by Rhinehart in conjunction with hot working of metals using explosive standoff operations [59]. Similarly, Ferreira and Shang have attempted to shock initiate admixed exothermic mixtures to locally enhance sample properties [53,54]. By eliminating the external furnace, the remotely controlled transfer system, used in HEC to move the heated powders from the furnace to the explosive assembly, is not needed. Furthermore, placing the heating source around the sample is also desirable since now the powder sample can be heated and consolidated in the same fixture.

The "chemical furnace" is a highly exothermic mixture of reactant powders that, when allowed to react, will generate heat and high temperatures. Such reactions can be classified under the broader classification of Combustion Synthesis, or Self-propagating High-temperature Synthesis (SHS) reactions. SHS involves the synthesis of products directly from their elemental precursors, via the propagation of a solid-solid combustion front through a green powder compact (e.g., Ti + C --> TiC). Once the process is initiated, the heat of reaction is sufficient to sustain the reaction until all of the reactants have been consumed. These reactions are characterized by reaction rates of 1 cm/s, temperatures of about 3,000° C, and the, sometimes violent, evolution of impurities trapped on the reactants. The potential advantage of the combustion synthesis process is that it requires little energy input and the processing time is reduced to seconds rather than hours. Further descriptions of the SHS process and its associated characteristics can be

found in DARPA/Army SHS Symposium Proceedings (1985), Munir (1988), and Combustion and Plasma Synthesis of High-Temperature Materials (1990) [60–62].

In LPS, the initial metal powder morphology is not important, since the W partially or completely dissolves into the matrix. A significant difference between LPS, HEC, and CSA-HEC processes is that, in the latter, the material to be compacted remains at high temperatures for only a short time. Specifically, in CSA-HEC, the short preheating cycle is followed by a rapid quench during densification. This inherent characteristic may be a critical advantage if the desirable properties, such as size distribution and morphology, of the precursor W are to be retained. Another aspect of quenching may be to reduce impurity segregation to interfaces or grain boundaries. Careful adjustments of the available heat and peak temperature achieved during preheating can limit the amount of sintering, dissolution, and melting in each phase to maintain the precursor W structure and morphology. That is, while some melting of the Ti matrix would be allowed, due to its much higher melting point the complete dissolution of the W could be prevented.

The primary objective of this research effort was to demonstrate that the CSA-HEC technique can be applied to fabricate high-density W-Ti alloys suitable for penetrator applications. The secondary objective was to identify the critical parameters for the CSA-HEC process. These included the effects of the amount of explosive charge, configuration and relative amounts of sample and chemical furnace, and post-compaction annealing. Other objectives including the control of peak temperature and heat conduction (rate of temperature rise) to and from the sample in this system were of interest. Similarly, the extent of intermixing between the precursors and changes in the initial precursor powder morphology was of concern. Finally, since in CSA-HEC the W-Ti sample is subjected to extremely large stresses and strains during the consolidation event, it was important to understand the effects, if any, of the rapid passage of the impulsive force on the microstructural properties of the material. The pertinent features of the technique and the properties of the W-Ti alloys produced will be described.

2. EXPERIMENTAL PROCEDURE

High purity (99.9%), 12-μm tungsten (Johnson Matthey, Ward Hill, MA, Cat. No. 10400), (99.5%) pure, −325 mesh (equivalent to −44 μm) titanium (Micron Metals, Gates City, UT, Cat. No. Ti-020), and (99.9%) pure, 2-μm graphite (CERAC Inc., Milwaukee, WI, Cat. No. 41A) powders were used to evaluate the CSA-HEC process. The precursor metal powders were examined by Scanning Electron Microscopy (SEM) (JEOL, Peabody, MA) and Energy Dispersive X-ray Spectroscopy (EDS) (Noran Instruments, Middleton, WI). It may be noted that the graphite powder was not subjected to the same scrutiny because it was used strictly to provide the required heat release via the exothermic chemical reaction.

The titanium and tungsten powders were ball-milled for several hours under argon atmosphere. A 95/5 (wt.%) W/Ti ratio was maintained in all of the experiments. The titanium and graphite powders with a Ti/C molar ratio of 1.0 were also dry-mixed and ball-milled under argon atmosphere. The titanium-carbon powder mixtures were uniaxially pressed at 44 MPa into several 100-mm outer diameter, 50-mm inner diameter, and 20-mm-thick, doughnut-shaped green compacts.

Figure 1 shows the CSA-HEC reaction vessel which functions not only to contain the Ti+C SHS reaction, but also as the die of the explosive compaction fixture. In this case, as in the usual planar die/anvil compaction configuration, the lid assembly of the reaction vessel serves as the matching anvil. The relevant components of this embodiment are: the mild steel reaction vessel, W+Ti powder sample, the doughnut-shaped Ti+C green compact, ZrO_2 (Zircar Products Inc., Florida, NY), and Grafoil (Union Carbide, Cleveland, OH) insulation, Ti+B igniter mixture, electric match, and the explosive driver package consisting of a set of high hardness steel anvils, aluminum piston (lid assembly), and the PVC container holding the powdered Amatol (80/20 NH_4NO_3/TNT) explosive (detonation velocity, v_d = 3,850 m/s), C-4 detasheet booster, and detonator. Because copious quantities of volatile impurities are released by the SHS reaction, vent holes were bored into the wall of the reaction vessel. The use of ZrO_2 thermal insulation was required to reduce heat losses from the reacting Ti+C compact and to protect the aluminum

7

piston/high hard steel anvil assembly and the explosives from overheating. The primary purpose of the Grafoil was to function as an inert barrier preventing the diffusion of contaminants into the sample, but it also eased separation of the compacted components. A reliable ignition system to initiate the SHS reaction was found in commercially available model rocket igniters.
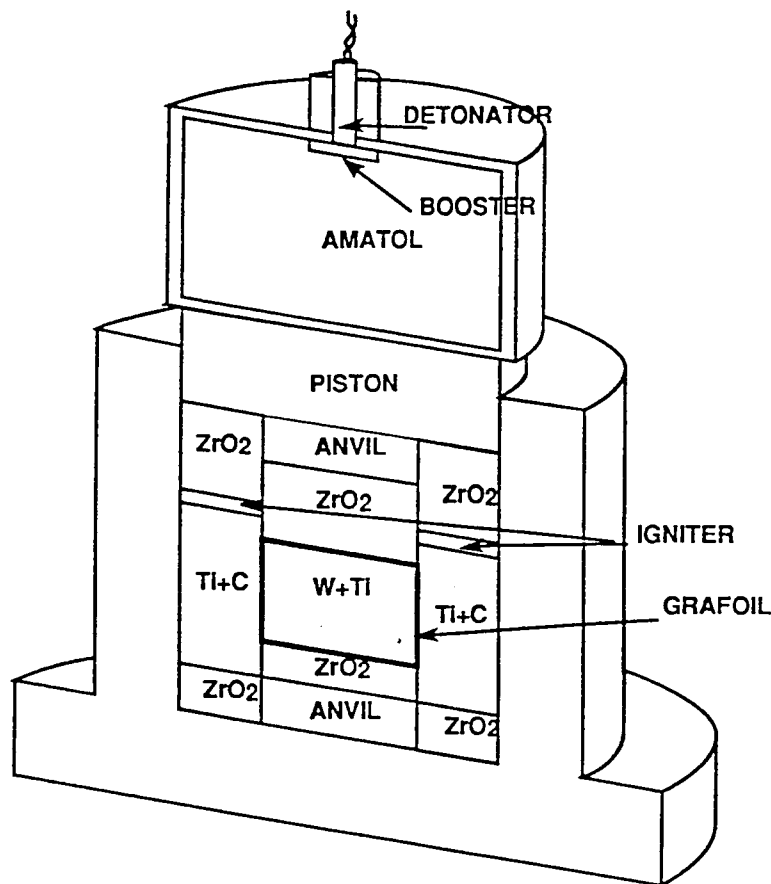
Figure 1. Schematic diagram of the CSA-HEC fixture used in the WTD HEC experiments.

Several aspects in the design of this reaction vessel/compaction fixture were based on those used in the explosive compaction of TiC and TiB_2 ceramics. In fact, much of the fabrication and assembly of components, as well as the experimental procedures, were similar to those followed in the above experiments. See Niiler et al. for additional details [63]. It is emphasized that the objectives in the TiC and TiB_2 experiments were to produce fully dense ceramics by the explosive compaction of the hot ceramics immediately after their formation via SHS. However, in the current HEC experiments the function of the ceramic was only to provide the heat necessary to increase the temperature of the sample.

Customarily, the reaction vessel and explosive container were readied separately. In short, the preparation of the two components were as follows. At the bottom of the reaction vessel, around the bottom anvil, porous ZrO_2 was placed to thermally insulate the Ti+C green compact. The inside surface of the Ti+C doughnut was lined with a thin sheet of flexible Grafoil insulation and the cavity filled with the powdered W+Ti sample. The approximate packing density of the powder was 50–60% T.D. Grafoil sheets were used to separate the top, bottom, and sides of the sample from the adjoining TiC and ZrO_2 insulation. The electric match, packed in loose igniter powder, was set atop the Ti+C green compact with its leads brought through one of the vent holes. Another layer of ZrO_2 insulation was placed above the Ti+C green compact, and, with the aluminum piston inserted partway into the cavity, the reaction vessel could be sealed. The explosive container was filled with oven-dried Amatol explosive. The packing density of this explosive was usually about 0.95 g/cm^3. The container's lid, with a small piece of detasheet attached to its underside, was fastened to the container, thereby completing the preparation sequence.

Prior to the experiment, the explosive container was affixed to the top of the aluminum piston and the completed assembly was placed on a 2–3-m-high sandpile. Once the detonator was in place, the electric match was remotely activated, which, in turn, initiated the igniter mixture and Ti+C green compact, and, as the TiC reaction proceeded to completion, normally in about 3 s, the enclosed W+Ti powder bed was heated to high temperatures. When a predetermined time had elapsed, the anvil was activated by the detonation of the explosive to densify both the sample and TiC furnace. The entire fixture was buried under sand that served to further protect the case and contents from thermal shock. After the fixture and its contents had cooled sufficiently, the W-Ti sample was extracted. The entire experiment was recorded on videocassette tape to determine accurately the reaction-detonation delay time, as well as any anomalies that may have occurred during the process.

To produce full density W-Ti samples, three key variables were considered: c/m (explosive charge mass to piston-anvil mass ratio), n_{TiC}/n_s (ratio of moles of exothermic compound to moles of sample), and, t_d (reaction-detonation delay time). In the primary optimization series, the c/m

ratio was varied from 0.4 to 2.6. The initial low c/m value was based on the experiments with TiC and TiB_2 ceramics to densify the sample without producing excessive cracking. In these experiments, the n_{TiC}/n_s was maintained at 6.3 ± 0.4. A secondary optimization was performed with c/m using a higher n_{TiC}/n_s of 8.6 ± 0.3. A few experiments were also conducted with the ratio of 3.2. Additionally, a series of auxiliary experiments was carried out for each n_{TiC}/n_s value to measure the sample temperature and rate of heating in the reaction/compaction fixture during the preheating phase of the process. For these experiments, the reaction/compaction fixture was modified by removing the explosive container and inserting, through the base of the fixture, a series of five W-5Re/W-26Re thermocouples into the middle of the tungsten-titanium powder sample. Two Chromel-Alumel thermocouples were also situated in the vessel, one near the electric match and another beneath the Ti+C doughnut, to mark the initiation and completion of the TiC SHS reaction. The block diagram of the modified reaction/compaction fixture with the lateral arrangement of the thermocouples is depicted in Figure 2. In these experiments, once the TiC reaction was initiated, the emf output of the thermocouples was recorded as a function of time by a PC driven, Metrabyte DAS-16 acquisition system until the fixture cooled to ambient temperature.

The effectiveness and uniformity of compaction of the W-Ti alloy samples were evaluated by density measurements and optical microscopy. The CSA-HEC samples were cut into several roughly equal sections with a diamond cutoff saw, and the mass density was measured with a water immersion technique. These density measurements revealed that the samples are compacted fairly uniformly with a density variation of about ±0.5%.

The central region of the CSA-HEC samples was further sectioned into thin, 1–2-mm wafers (parallel to the compaction direction) in an Electric Discharge Machine (EDM) (Metals Research Group, Monseyn, NY) for SEM, X-ray Diffraction (XRD) (Philips Electronic Instrument, Mahwah, NJ), and Transmission Electron Microscopy (TEM) (Philips Electronic Instrument, Mahwah, NJ) analyses. The wafer selected for the XRD sample was first polished to remove any EDM induced surface damage, sectioned to fit, then epoxy-mounted into standard aluminum

10
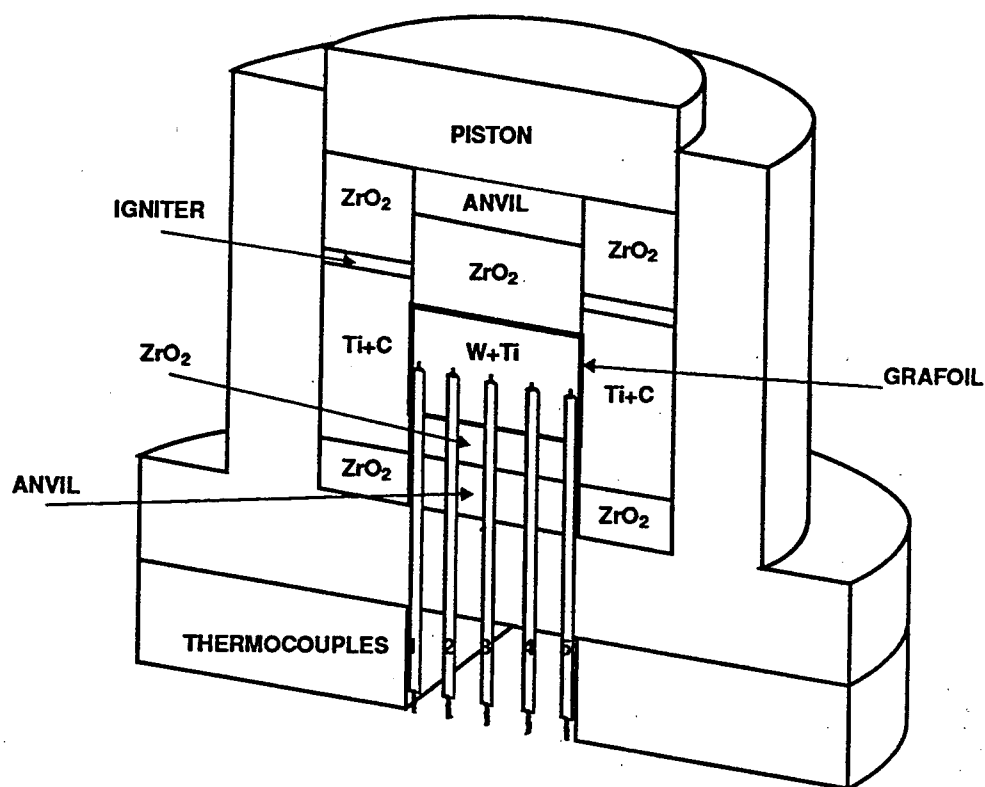
Figure 2. Schematic diagram of the modified reaction fixture used in the precompaction sample temperature measurement.

Philips X-ray diffractometer sample holders. The XRD samples were scanned through a 2 theta range of 20–120° using a 0.025° increment and a 5-s dwell time.

The SEM samples were mounted in a thermosetting, glass fiber filled, diallyl phthalate resin and polished to a 1/4-µm finish. Because of the great difference in the relative hardness of tungsten and titanium, a special procedure had to be developed to obtain the true microstructure of the W-Ti samples. In particular, this methodology required the use of a combination polishing/etching sequence during the final polishing step. First, the samples were plane ground with SiC to a 5-µm finish, followed by diamond polishing to a 1-µm finish. At this stage, the underlying structure of the sample was hidden by the fact that the titanium phase tended to smear onto the nearby tungsten phase. The final polish was performed with a chemically resistant cloth

11

and an alkaline-based (pH 9.8) 0.05-µm silica suspension (Struers, Inc., Cleveland, OH) until the true structure was revealed.

The polished cross-sections were examined with SEM and EDS for grain morphology and structure. Fracture surfaces from the W-Ti samples were generated by impact loading and examined for a qualitative evaluation of the degree of intergrain bonding. Furthermore, microhardness measurements were performed using a Vickers indentor with a 100-g load. Quoted hardness values are averages from at least 10 individual hardness measurements.

Several wafers, cut from a typical CSA-HEC sample, were vacuum annealed at 700, 1,000, or 1,400° C. A heating rate of 5° C/min was used to reach the respective soak temperature. The samples were soaked for 24 hr, slow cooled at 5° C/min to 200° C, and allowed to furnace cool to room temperature.

Of the entire sample analysis procedure, the preparation of the TEM specimens proved to be the most time consuming. The TEM samples were prepared by first reducing the 1-mm-thick wafer, cut by EDM earlier, until its thickness was about 100 µm. This was accomplished by sequentially polishing one side of the wafer, then the other, to remove the EDM induced damage. Once at the desired thickness, about 0.1–0.2 mm, a 3-mm-diameter disk was cored out of this blank using the EDM. These disks were further thinned by dimpling until the thickness at the center of the disk was less than 30 µm. Finally, the dimpled disk was ion milled in a Gatan 600 dual-stage ion mill at 6 kV with an 11° gun tilt until the center was perforated. Though conceptually straightforward, the entire TEM procedure was tedious, especially the dimpling and milling steps, and required extreme care as almost all of the W-Ti samples were very brittle and highly susceptible to cracking. Additionally, it may be noted that in the preparation of the TEM samples, the preliminary steps were done in-house, however, the dimpling and ion milling were done at the University of Delaware.

3. RESULTS AND DISCUSSION

The W-Ti equilibrium phase diagram is shown in Figure 3 [11]. The pertinent features of this system include a critical point at 1,250° C, 33W-67Ti (at.%), corresponding to the beta-Ti,W <-> beta-Ti + W reaction, and, the beta-Ti,W <-> W + alpha-Ti monotectoid reaction at 740±20° C, 9W-91Ti (at.%). Above the critical temperature (indicative of a miscibility gap), a complete range of beta-Ti,W solid solutions exists. For W contents lower than 6 at.%, the bcc beta-Ti,W structure cannot be retained and instead the martensitic cph phase alpha', or its orthorhombic distortion, alpha'', results upon quenching. A table containing molecular weights and densities (physical mixture calculation) for a range of W-Ti alloy compositions is furnished in Appendix B.

A quick survey of Appendix A reveals that past applications of HEC were limited to homogeneous systems such as pure and prealloyed metals and ceramic powders. Nevertheless, it was hypothesized that the extension of HEC to the heterogeneous W-Ti alloy system would be straightforward. In a binary system, using the procedures of Gorobtsov and Roman, the relatively long preheating phase would most likely allow the dissolution of W to form a beta-Ti,W solid solution. Much like in a quench, during the rapid cool-down following the explosive compaction event, this structure would likely be retained. In the CSA-HEC variant, the length of the heating phase is greatly reduced, therefore, it was expected that the beta-Ti,W solid solution would be predominantly limited to interfacial regions leaving the original W grain morphology unchanged.

Adiabatic heat balance computations were performed in the 95W-5Ti (wt.%) system to determine the required amount of chemical furnace; i.e., a baseline value. It may be noted that these calculations did not consider heat losses or geometrical constraints in the reaction/compaction fixture. Results indicated that, an n_{TiC}/n_s ratio of 1.0 would cause the Ti component to melt.
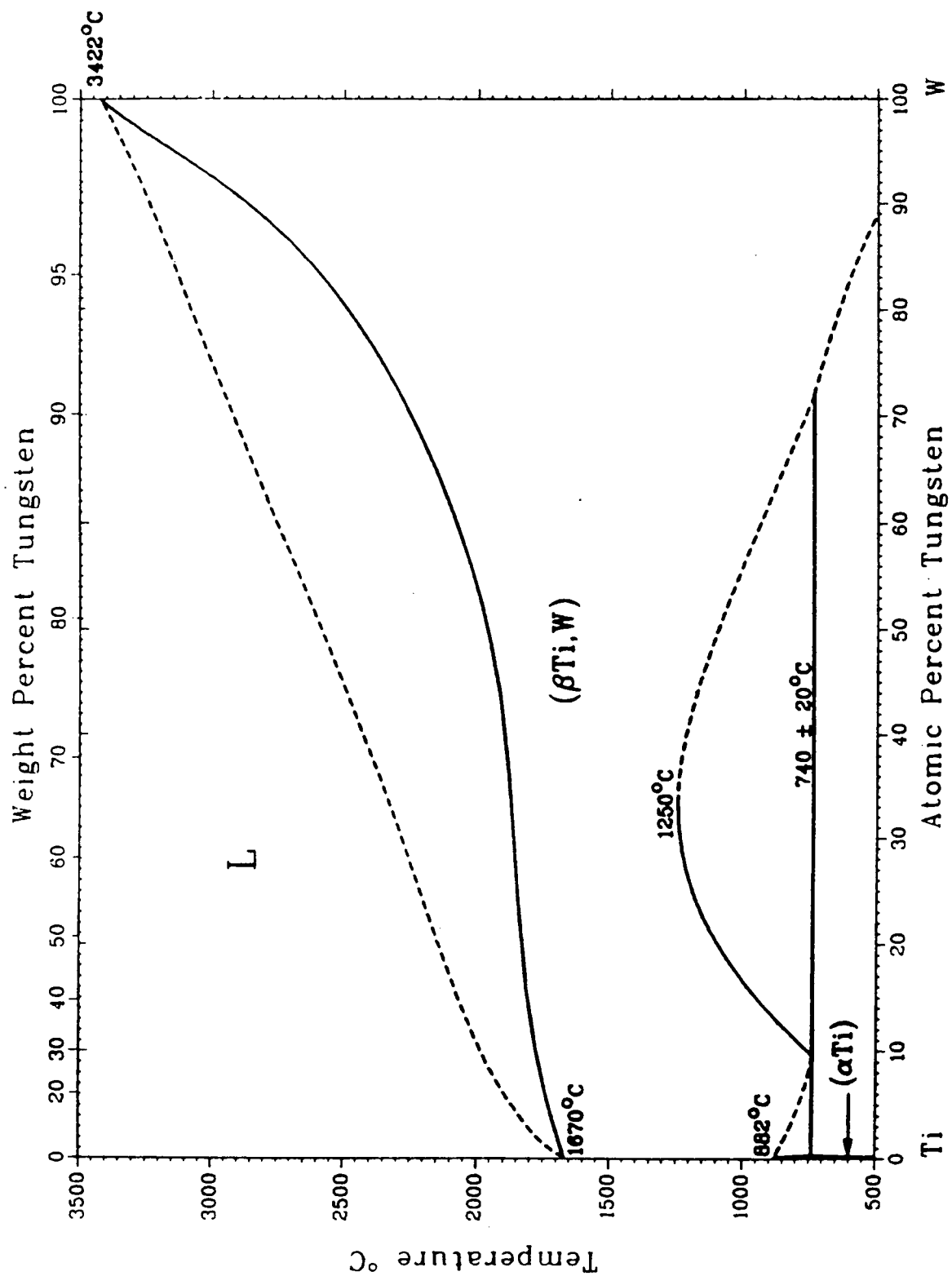
13

Figure 3. Equilibrium phase diagram of the tungsten-titanium system from Massalski [10].

14

Preliminary configurational experiments determined that placement of the TiC chemical furnace in a concentric geometry is most suitable for uniform consolidation. Compactions using layered and complete envelopment geometries were not entirely successful in the simultaneous ignition of the chemical furnace, resulting in nonuniform sample densities.

SEMs of the precursor powders and their respective polished cross-sections are shown in Figure 4. As shown in Figures 4A and 4C, the tungsten particles are either blocky or spheroidal, ranging in size from 10–20 µm, sometimes forming extensive agglomerates. In contrast, in Figures 4B and 4D, the titanium particles are irregular in size and shape, ranging from 20–30 µm and vary from blocky to highly elongated shapes. Consistent with the expected level of purity, bulk analysis using EDS detected no foreign contaminants.

3.1 Auxiliary Temperature-Time Measurement. The results of the auxiliary measurements of the sample temperature during the preheating phase were essential for the successful consolidation of the W-Ti samples. The experimental data for the n_{TiC}/n_s values of 3.2, 6.3, and 9.1 are presented in Figure 5. The temperature-time trace for 3.2 appears in Figure 5A, for 6.3 in Figure 5B, and for 9.1 in Figure 5C. Additionally, the temperature-time trace at the interior of the sample is shown on an expanded scale in Figure 5D. In the lower left-hand corner of each of the plots of Figures 5A, 5B, and 5C, the pair of vertical arrows marks the initiation and completion of the TiC SHS reaction. As expected, with an increasing amount of TiC, the duration of the reaction (i.e., the length of the heat pulse) correspondingly increases. In all three cases, the temperature at the samples' edges rises rapidly to reach a broad peak, drops, goes through a plateau, then, due to continued heat losses, steadily decreases. As the heat pulse travels inward to the sample's center, the temperature profile is changed. A more sluggish rise in the temperature and the absence of the peak results in the wide plateau and subsequent decline only. Thus an immediate feature of the data is the fact that the periphery of the sample undergoes a different thermal history than its midregions.

As seen in Figure 5A, for $n_{TiC}/n_s = 3.2$, the temperature is 1,500° C at one end of the sample, and is near T_m Ti = 1,670° C, at the other. The temperature at the sample's center is only
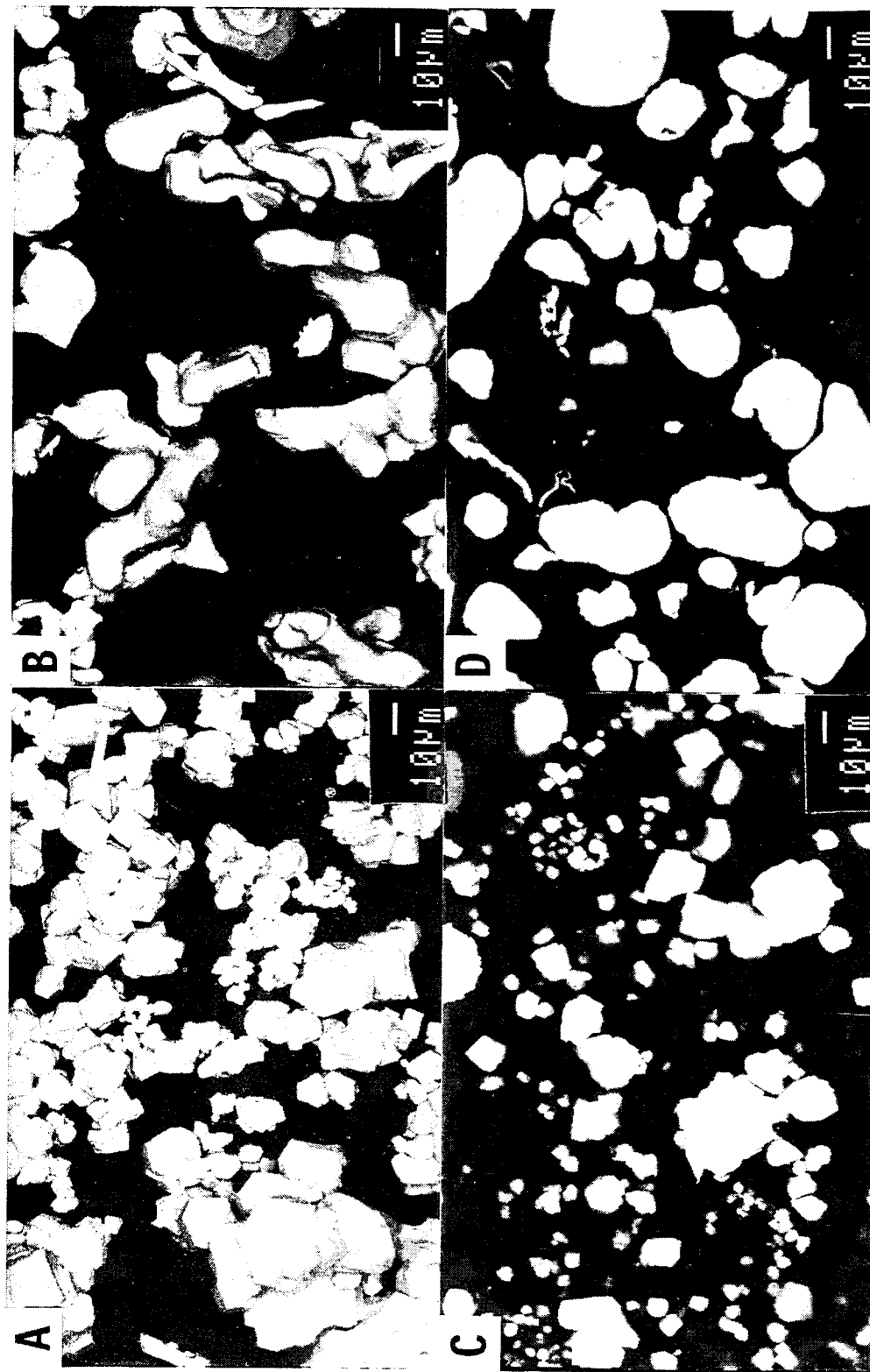
Figure 4. Secondary electron micrographs of the precursor powders. The tungsten powder is shown in 4A, the titanium powder is shown in 4B, the polished cross-section of the tungsten powder in 4C, and the polished cross-section of the titanium powder in 4D.

16
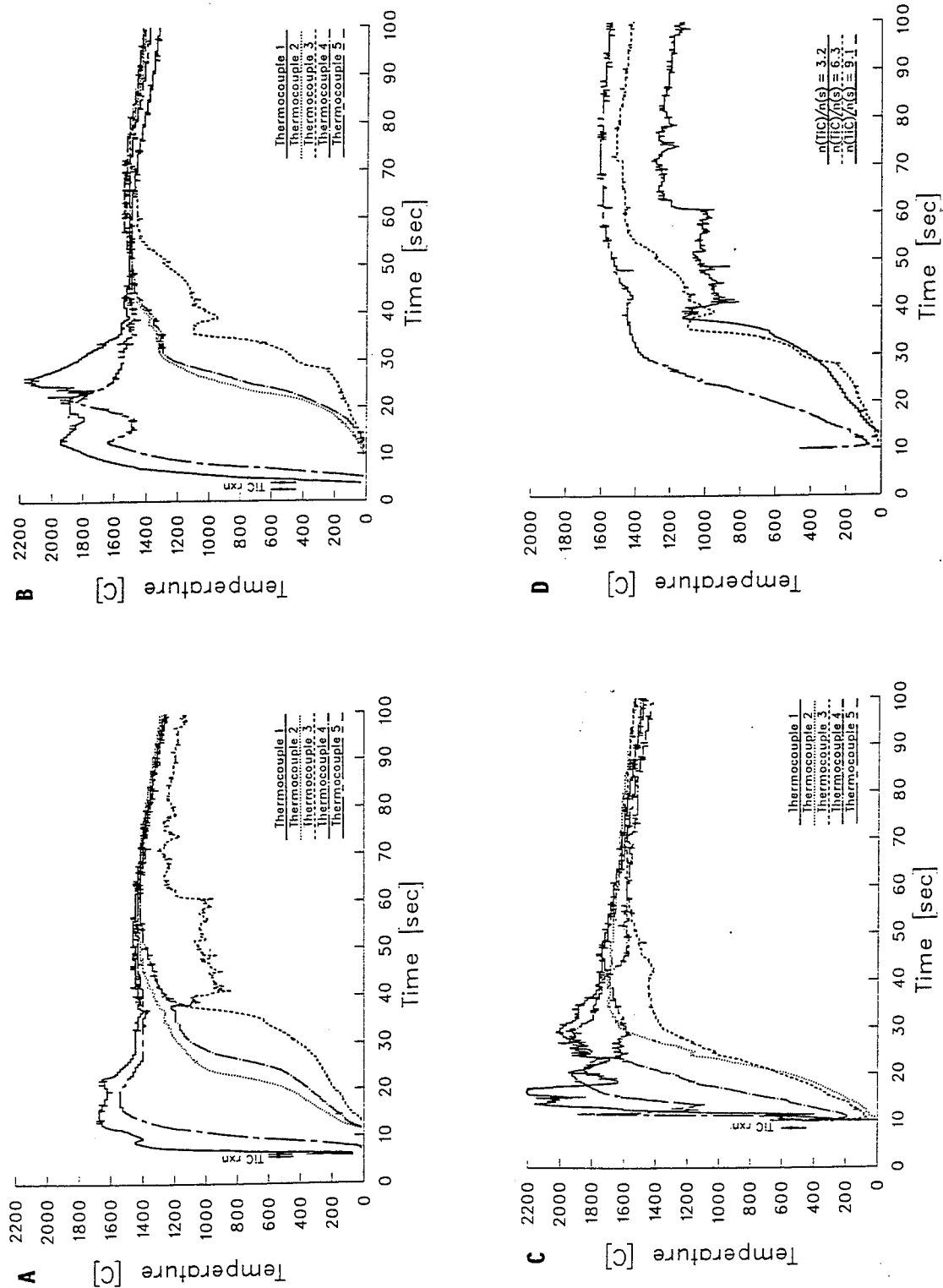
Figure 5. Temperature data for the sample with an $n_{TiC}/n_s = 3.2$ is shown in 5A, for an $n_{TiC}/n_s = 6.3$ in 5B, and for an $n_{TiC}/n_s = 8.3$ in 5C, and the interior temperature for all three n_{TiC}/n_s in 5D.

1,250° C, well below T_m Ti. For n_{TiC}/n_s = 6.3, the temperature at the outer edge of the sample reaches 1,900° C at one end and 2,100° C at the other. See Figure 5B. In this case, the sample's center temperature is higher, reaching 1,550° C, but does not exceed T_m Ti. Finally, in Figure 5C, for n_{TiC}/n_s = 9.1, the sample reaches temperatures well above 2,400° C at its periphery and 1,650° C at its center. Although the heating rates (note the temperature rise in the curves) for the two smaller n_{TiC}/n_s values are similar, in the last case it is markedly different. Specifically, the temperature rise at the sample's interior is more rapid, much like that of the periphery. In the two cases with larger n_{TiC}/n_s values, the critical aspect of the data is that at approximately 60 s after the initiation of the TiC reaction the sample becomes isothermal. In the case with n_{TiC}/n_s = 3.2, the sample never reaches an isothermal plateau and continues to suffer from severe temperature gradients.

The temperature-time data presented above reveals that the n_{TiC}/n_s significantly affects the heating rates and peak temperatures attained within the sample. Even at the small n_{TiC}/n_s = 3.2, the temperature at the sample's edge nearly reaches the melting point of Ti. A threefold increase of n_{TiC}/n_s results in a 1,000° C increase in the sample's edge temperature. The sample's center is less sensitive to this change, since the interior temperature varies only by about 400° C. Ideally, for best compaction results, the n_{TiC}/n_s should be adjusted such that as much of the bulk of the sample is near, but does not exceed the T_m Ti, and the excessive overheating of the periphery is minimized. However, unless a large enough n_{TiC}/n_s is used, the sample will not become isothermal at any point during the preheating cycle. The n_{TiC}/n_s = 6.3 satisfies both of these criteria.

After cooling, the uncompacted W-Ti sponge from the n_{TiC}/n_s = 6.3 test was sectioned and the degree of intermixing and interparticle wetting evaluated. Figure 6 shows the cross-sectional profile of the W-Ti sponge. The sponge is not quite uniform in thickness, and its walls curve inward. Usually the interior of the sponge has a uniform gray color with some minor blooming (appears darker gray) at its periphery. Based on the temperature data, it is believed that the discoloration is caused by overheating of the periphery. Sometimes, as is apparent, the sponge contains a few fissures. It will be demonstrated that these flaws are healed by the compaction

18

process. An SEM photomicrograph of the sponge's core region and associated EDS dot maps of Ti and W of the corresponding substructure are shown in Figures 7A, 7B, and 7C. In the image, the lighter gray particles are tungsten, the darker gray particles are titanium, and the dark background is the nonconductive epoxy filler of the mounting compound. Overall SEM examination of the sponge reveals that the distribution of titanium particles among the tungsten aggregates is isotropic and uniform. Locally, as the SEM image in Figure 7A illustrates, during preheating, the titanium spreads around nearby tungsten grains. The well-defined edges of the W particles surrounded by Ti are suggestive that solid solution formation between Ti and W is limited. Nevertheless, it must be kept in mind that the frictional heating between the particles that occurs during consolidation may bring about some localized melting, furthering solid solution formation.
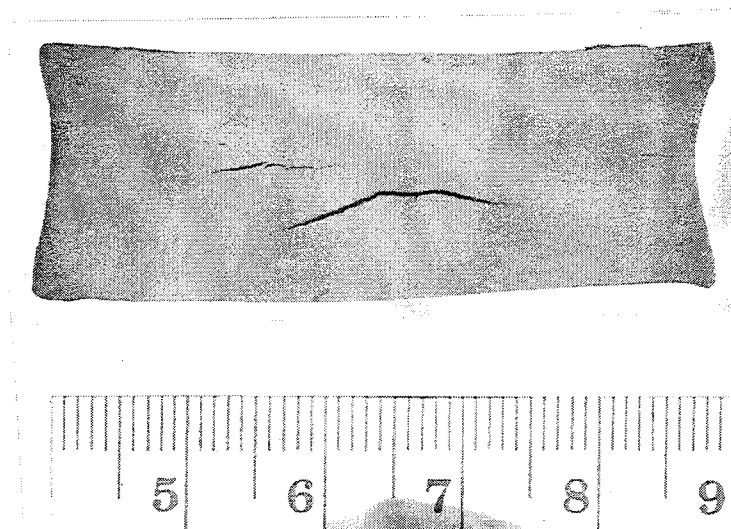
Figure 6. Microphotograph of a typical uncompacted W-Ti sponge with an $n_{TiC}/n_s = 6.3$.

3.2 HEC Experimental Program. The CSA-HEC samples were approximately 9-mm thick with a diameter of 50 mm. A photograph showing the top, bottom, and side views of a typical sample is presented in Figure 8. In the side view, the two halves of the cut sample are placed bottom to bottom. The top surfaces of the samples were mostly flat, while the bottom surfaces were slightly convex. The sides of the samples were often rumpled, ranging from very fine to coarse textured striations and creases. The edge of the samples usually contained minor annular and radial cracks that extended into the outer 5-mm periphery only. However, no evidence of horizontal hairline cracks were found in the hot explosively consolidated samples. Occasionally,

some of the samples suffered from a random network of vertical hairline cracks. After sectioning such samples, the cracks were seen to occur along diagonals, originating at the top or bottom sample surface and terminating at the sides. Most likely, these cracks are caused by the reflection of the compressive wave from the free surfaces of the fixture during the consolidation event.

3.2.1 Results of Density Optimization. Results of the experiments to increase sample density by varying c/m and n_{TiC}/n_s are shown in Figures 9A and 9B respectively. As apparent in Figure 9A, the density initially increases with the c/m for both n_{TiC}/n_s values; however, above a certain saturation value, there is a decrease in the sample density. Most likely, at higher c/m values, the combination of the increasing shock duration and rarefaction waves induces delaminations and cracking, thereby damaging the sample. A maximum density of 98.9%T.D., with an $n_{TiC}/n_s = 6.3$, is reached at a c/m of 1.86. The density dependence with $n_{TiC}/n_s = 8.5$ parallels that of 6.4. Based on the maximum density of 97.0%T.D. reached at a c/m = 2.11, full-density is expected, i.e., above 98.0%T.D., at a c/m value of about 2.5. Also included are data from samples that were compacted with delay times much shorter than the time needed to reach the isothermal condition. Note that a 4-5% drop results if the sample is not at uniform temperature. To further improve sample densities, the density dependence with n_{TiC}/n_s was examined as well. In contrast to the data presented in Figure 9A, the sample density monotonically decreases with increasing n_{TiC}/n_s as shown in Figure 9B. It is speculated that during the consolidation event, at higher n_{TiC}/n_s values, the interior porosity of the sample is trapped by the excessively plastic outer zone, causing exit routes to be closed.

Optical microscopy of transverse and longitudinal cross-sections (with respect to the compaction axis) revealed a preferentially oriented two-phase structure. The distribution of the primary and secondary phases was isotropic in the transverse view; however, both phases tended to be elongated along a transverse plane in the longitudinal view. This appearance is consistent with stage-two compaction wherein grains deform plastically without exceeding the breaking stress in the powder body. EDS analysis of the samples showed that the primary phase consists of W only and the secondary matrix phase is a Ti-rich solid solution of Ti and W. During the
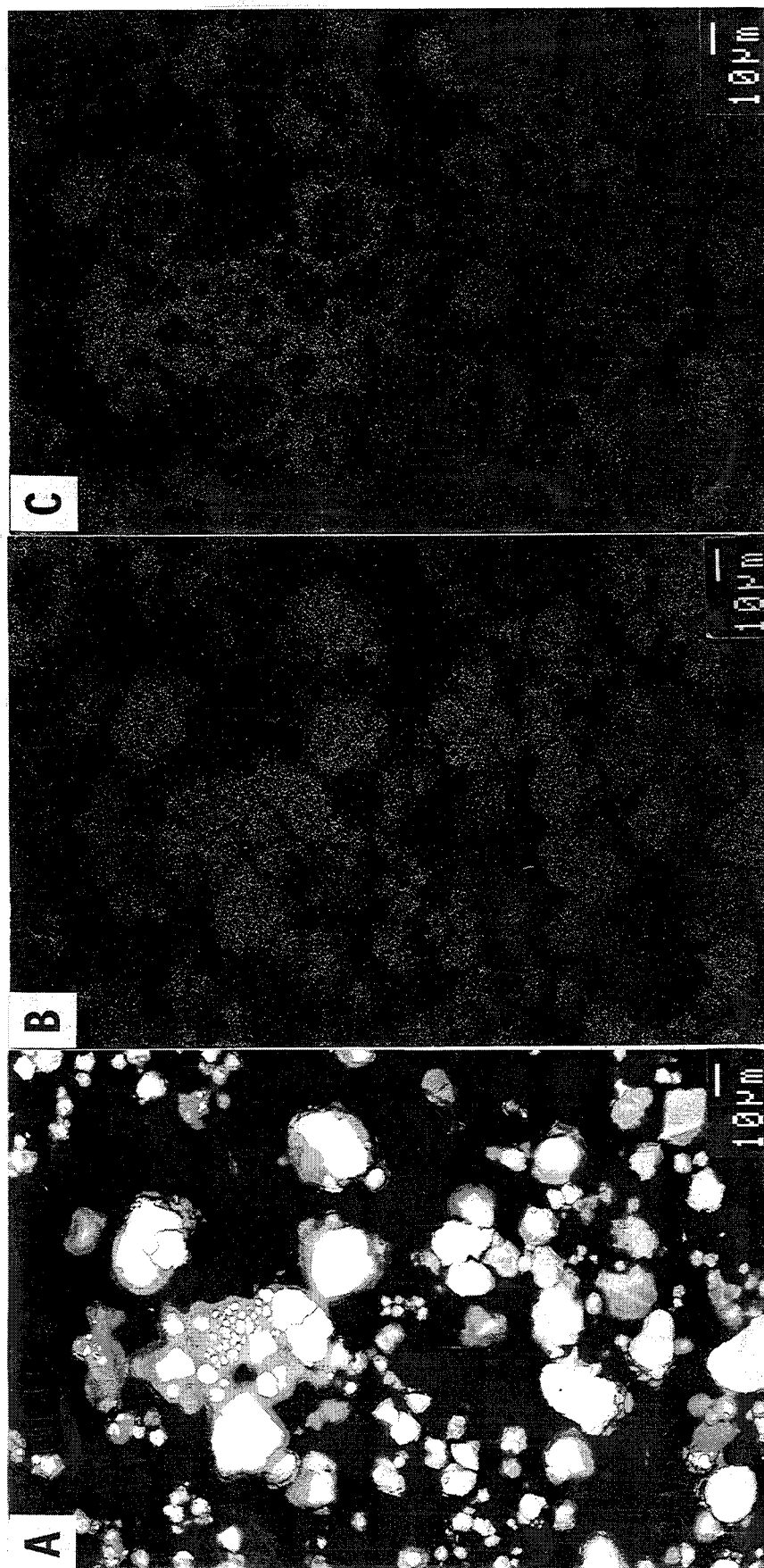
Figure 7. Scanning electron micrograph of the W-Ti sponge in 7A, EDS dot map of tungsten in 7B, and EDS dot map of titanium in 7C.
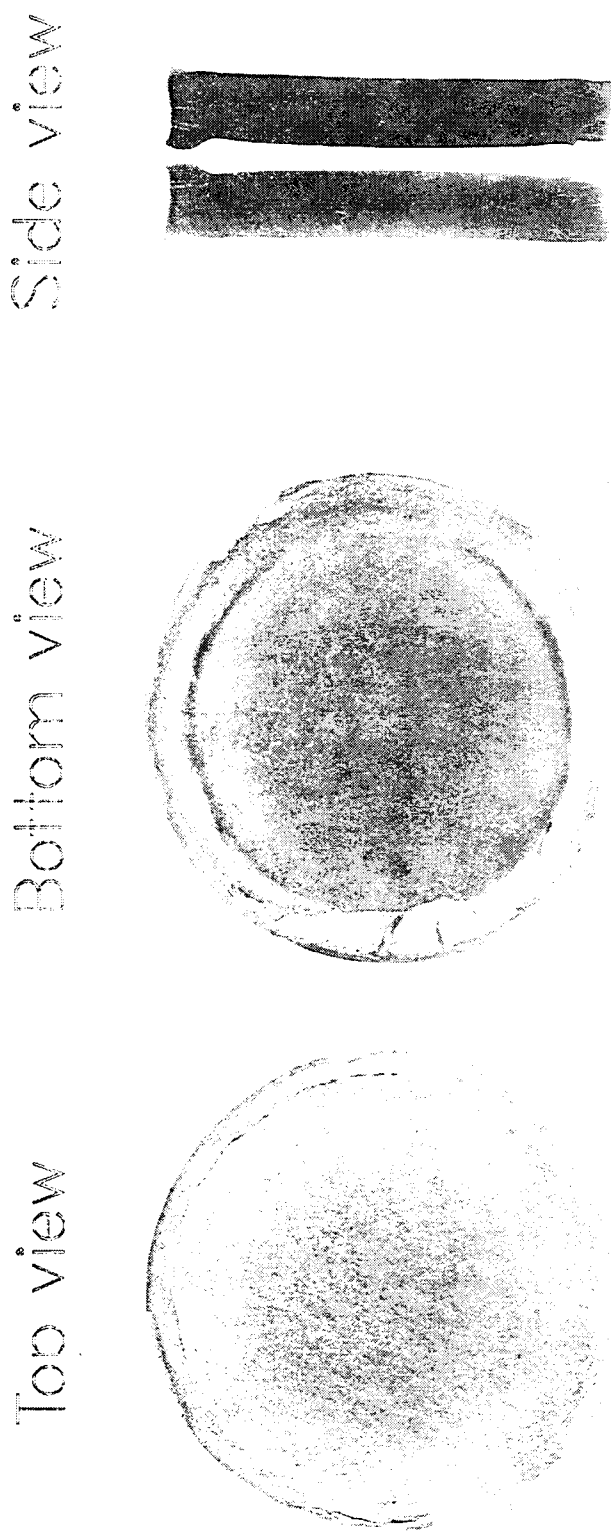
Figure 8. Microphotograph of a typical CSA-HEC sample showing top, bottom, and side view (sectioned sample placed bottom to bottom).
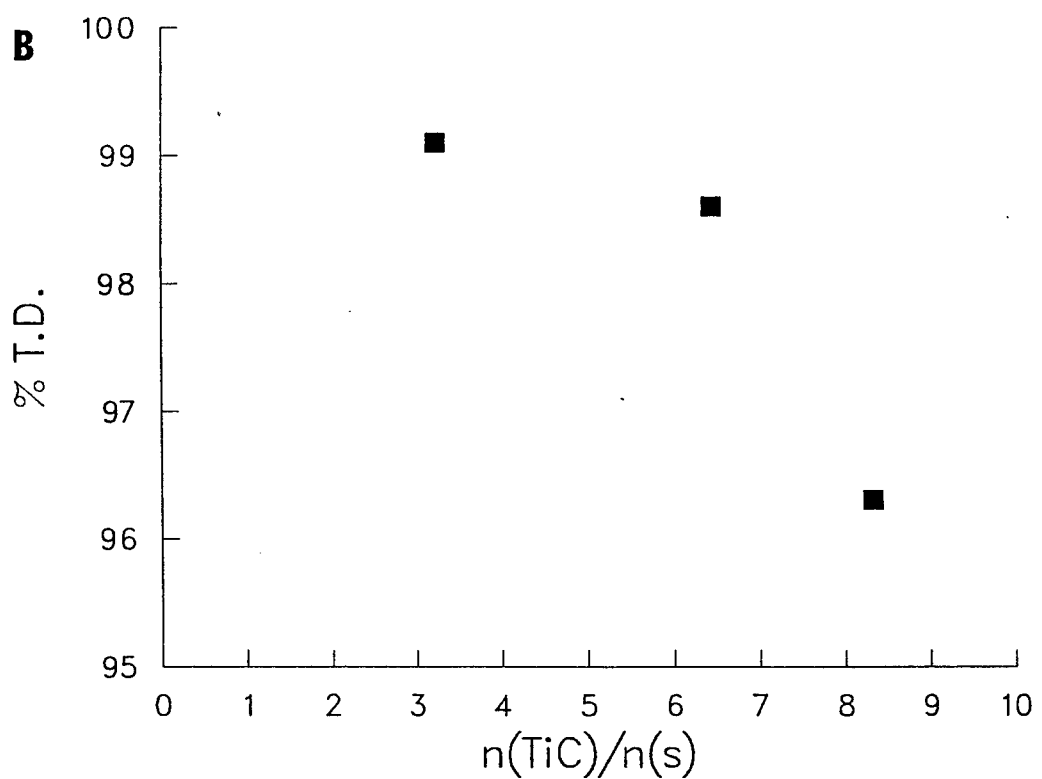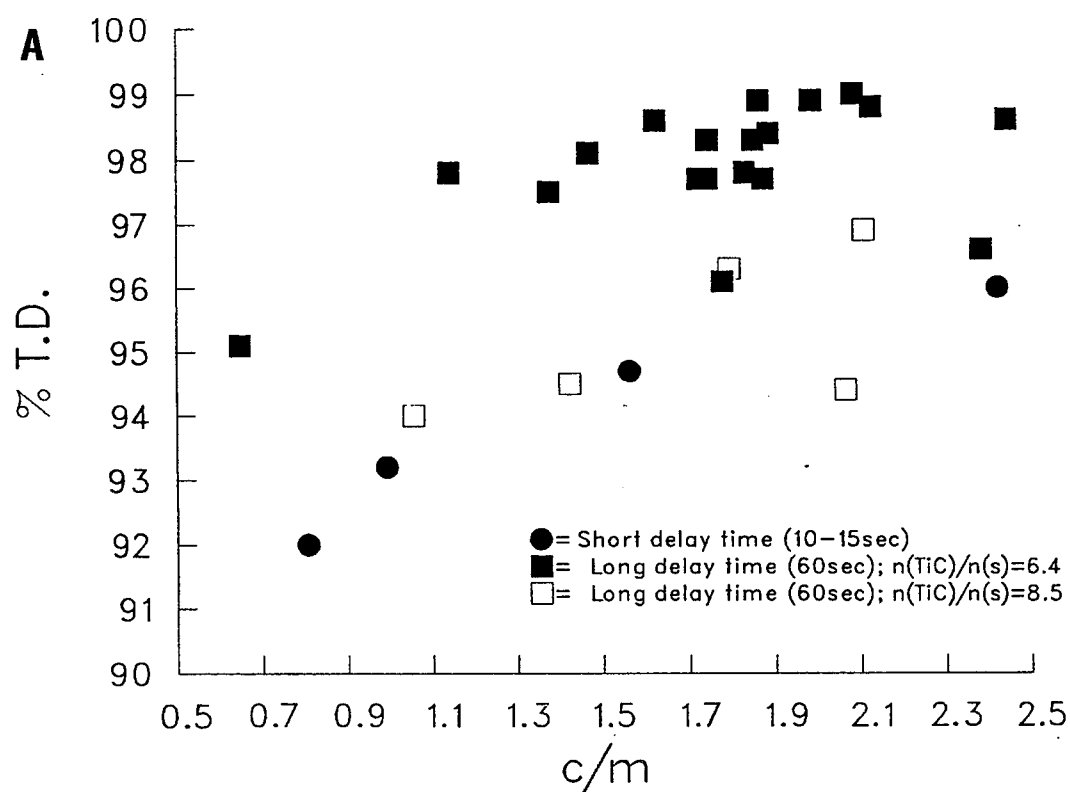
Figure 9. Sample density as function of c/m in 9A and n_{TiC}/n_s in 9B.

23

course of these analyses, no other elements were identified in the W-Ti samples. The presence of the W and Ti-rich phases was verified by XRD analysis. As seen in Figure 10, only the peaks corresponding to body-centered cubic W can be clearly recognized. Due to the relatively small amount of Ti-rich matrix phase in the 95W-5Ti (wt.%) samples, only the (110) diffraction peak, appearing on the shoulder of the (110) W peak, can be seen. It may be noted that the W peaks are not shifted indicative of little or no deformation of the crystal lattice. Other minor peaks are a result of the Al sample holder.

3.2.2 Microstructural Characteristics. Polished, longitudinal cross-sections from the core, transition (intermediate), and edge regions are shown in Figures 11A, 11B, and 11C for a typical sample. Additionally, shown in Figure 11D, a sketch of the sample's longitudinal cross-section depicts the relative extent of each of the regions delineated above. Lastly, Figure 11E exemplifies the typical substructures encountered in the W-Ti samples and the associated terminology describing them hereinafter. As seen in Figure 11A, the SEM micrograph (backscattered electron image) of the core region of the sample reveals a structure consisting of loose W grain aggregates (light gray) bounded by a partially continuous Ti-rich matrix (dark gray). As shown in Figure 11D, the extent of the sample core comprises a disk with a radius of about 19–20 mm. As indicated by arrows in Figure 11A, in some instances the Ti-rich phase is found to extend into the W aggregates. The Ti-rich phase contains an equiaxed grain structure with an average size of 5–10 μm.

Using semiquantitative EDS analysis, the W grains contained in the aggregates have a W content over 99 (at.%), and the Ti-rich phase has a composition of about 20W-80Ti (at.%). The micrograph from the intermediate region of the sample (see Figures 11B and 11D) reflects a significant shift from this morphology caused by higher local temperatures of about 1,800° C. This annular region, surrounding the core, is approximately 3–6 mm inward from the edge of the sample. Unlike the relative homogeneity of each phase observed earlier, as seen in Figure 11B, intermixing of W and Ti is more extensive and heterogeneous. The intensified dissolution of W grains can be noted in the appearance of a continuous W-rich solid solution surrounding W grain remnants. Observed mainly in the Ti-rich matrix phase, examples of heterogeneous, nonequilibrium

24
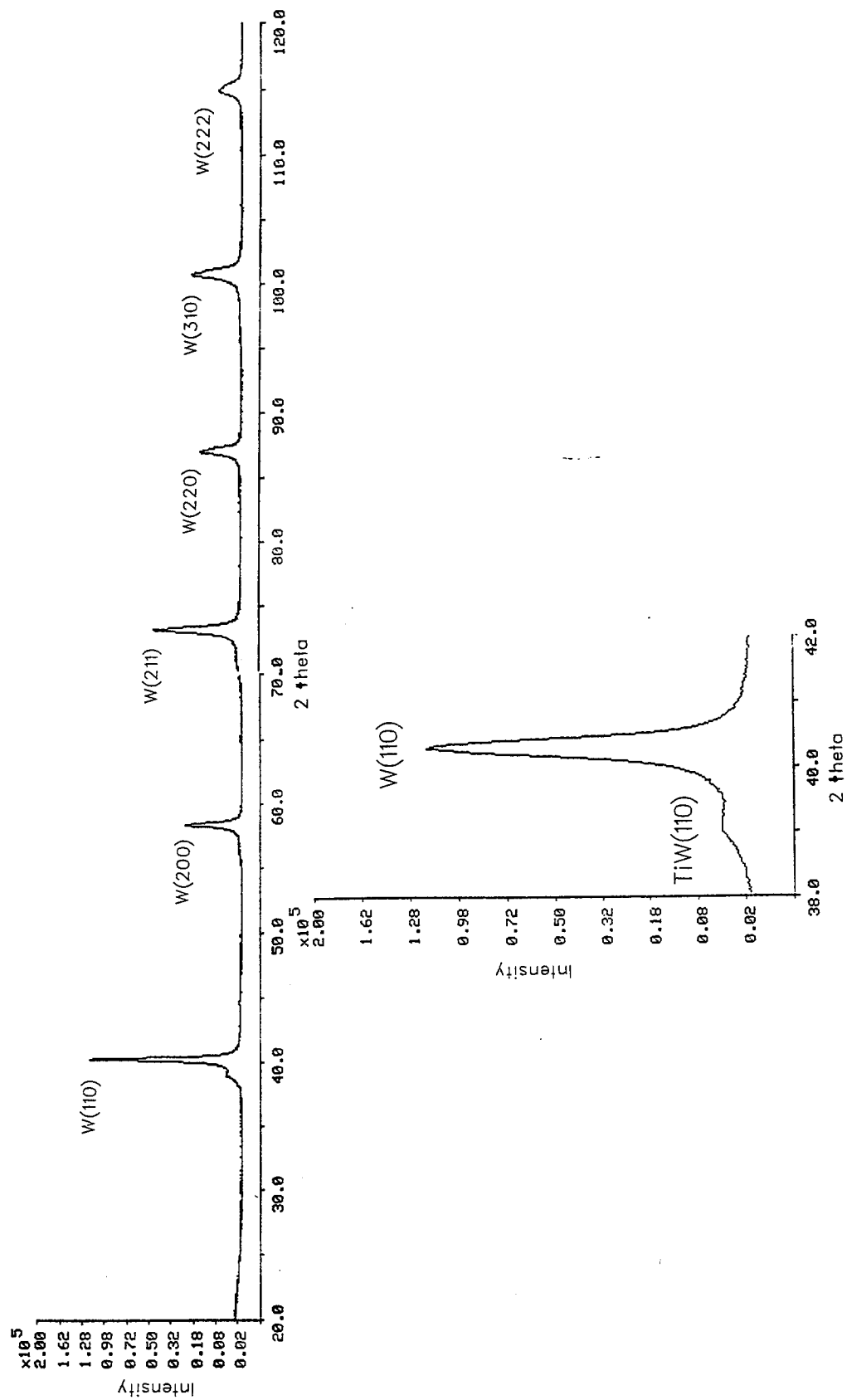
Figure 10. X-ray diffraction spectrum for a typical sample. Inset shows enlarged view of the (110) intensity peak at 2 theta = 40.4.
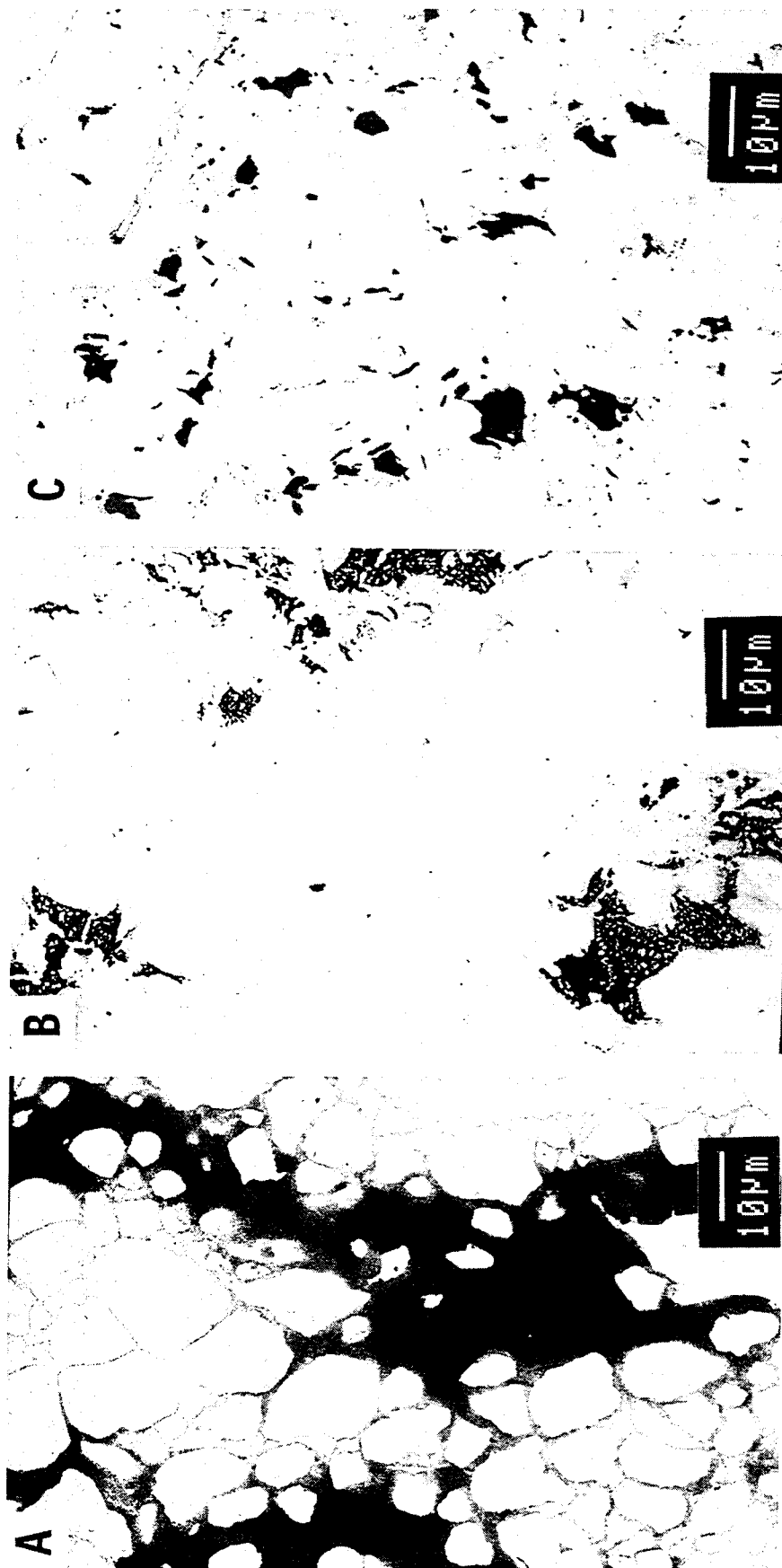
Figure 11. Backscattered electron micrographs of polished surfaces of a full density W-Ti sample ($n_{TiC}/n_s = 6.3$). Core region is shown in 11A, intermediate region is shown in 11B, and edge region is shown in 11C.

D

Edge region

Edge region

Core region

Intermediate region

Intermediate region

cm 1 2 3 4 5

E

Ti-rich matrix

W grain

W grain

duplex structures

precipitates

W-rich solid solution

10μm
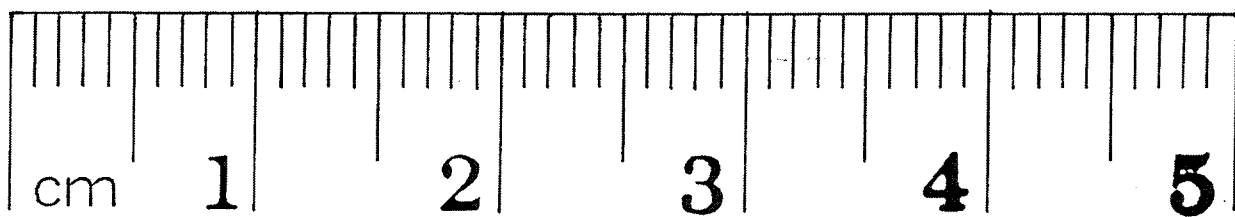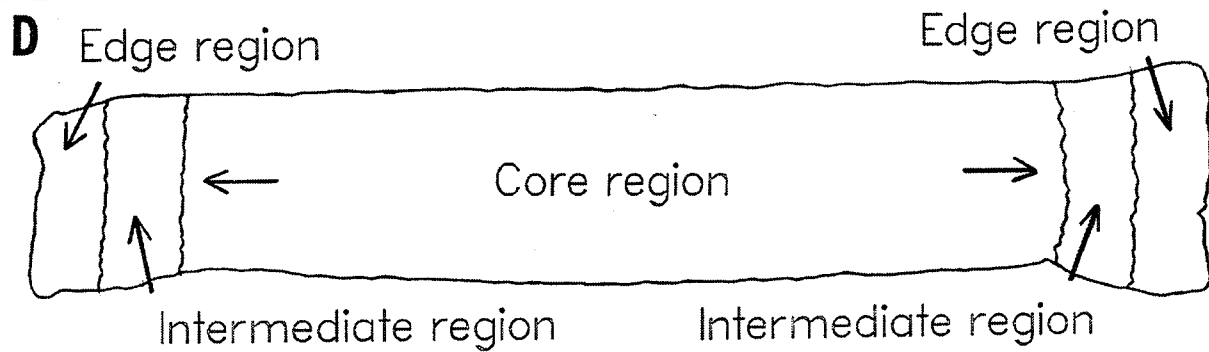
Figure 11 (Continued). <u>Spatial locations of the three regions are shown in 11D.</u> Typical substructures encountered in the samples and their associated nomenclature are shown in 11E.

partitioning include submicron precipitate clusters, micron-sized grain-boundary precipitates, and eutectoid-like duplex structures. Results of EDS analyses show 30W-70Ti (at.%) for the Ti-rich phase and 70W-30Ti (at.%) for the W-rich phase. Closer examination of the immediate vicinity surrounding precipitates shows 50W-50Ti (at.%) for the precipitates and 25W-75Ti (at.%) for the adjacent Ti-rich region.

Lastly, the edge region, or the outer 3-mm annulus, of the sample (see Figures 11C and 11D) exhibits the thermally most active state between the two components. It may be recalled that the temperature at the sample's edge is near, or above 2,000° C. In this region, the original W grains have mostly dissolved to form an interconnected W-rich solid solution, leaving the Ti-rich phase in small, isolated islands only. EDS of this region revealed 80W-20Ti (at.%) for W-rich areas and 5W-95Ti (at.%) for the Ti-rich islands. It may be noted that in the latter figures the W grains and Ti-rich regions have much straighter edges, indicating plastic deformation as well.

SEM examination of the samples with the lower and higher n_{TiC}/n_s values reveals a generally similar, oriented structure. At the lower ratio (3.2), the Ti-rich phase is practically discontinuous and intermixing is limited to the periphery of the W aggregates. In this sample, the EDS analysis of the Ti-rich phase indicates Ti contents similar to that of the standard sample with an $n_{TiC}/n_s = 6.3$. Similar morphological transition regions, as described previously, exist from the edge to the core of this sample. Their extent, however, is spatially narrower and located closer to the sample's edge. In contrast, at the higher ratio (8.5), the W aggregate breakup in the sample is more extensive, resulting in the improvement of Ti-rich matrix's continuity. Additionally, because of the higher temperatures in the latter case, the morphological transition from the edge of the sample to its core is wider, and the corresponding regions are located further inward, toward the sample's center.
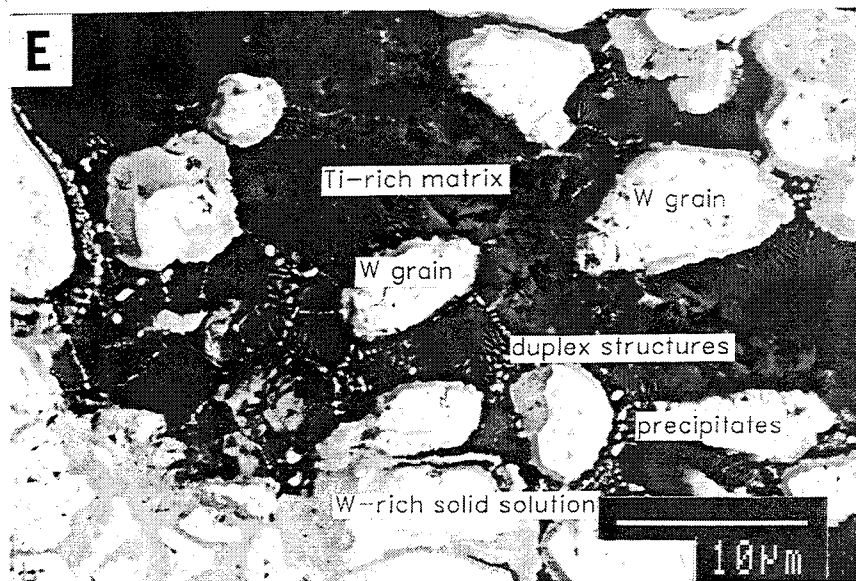
The various aspects of the sample's microstructure, shown in the Figure 11, can be delineated into the three distinct categories of preferential orientation, incomplete dispersion of Ti, and spatially dependent substructure of the matrix. While the first is influenced by a single factor, the others are determined by a variety of factors. The preferential orientation of the Ti-rich

regions simply arises during the uniaxial collapse of the W-Ti sponge. That is, when the initially isotropic mixture is compressed, the more plastic Ti will tend to deform and elongate to fill voids around the much stiffer W particle aggregates. Because extended sintering, and hence the possibility of redistribution, is prevented by the rapid cooling in the fixture, a fibrous structure results.

The incomplete dispersion of Ti in the sample is probably brought about by the considerable size difference, the relative melting points of the precursors, and the temperature at the time of compaction. Specifically, even at smaller n_{TiC}/n_s values, though moderately plastic, because of its larger initial size and its inability to flow extensively, the Ti cannot spread uniformly between the W grains. With an increasing n_{TiC}/n_s, and thus higher sample temperatures closer to T_m Ti, the ability of Ti to spread beyond the nearby W aggregates increases, causing their dispersion and breakup, thereby creating a more uniform and continuous matrix surrounding the W particles. However, an added effect of the increased mobility of the Ti will cause the associated rise in the degree of intermixing between the W and Ti components in the matrix itself and at the W grain/matrix interface.

The intermixing of the W and Ti may not be detrimental to the alloy but, most likely, unless the affected regions could be avoided or eliminated, the noted segregation and heterogeneity of the sample's microstructure will result in nonuniform properties. Nevertheless, the pronounced shift in morphologies can be understood by a careful examination of the heating and cooling cycle of each region of the W-Ti alloy. A possible explanation of the observed microstructures is offered below.

During the heating phase, the temperature of the outer edge of the sample rapidly rises well above the T_m Ti crossing the solidus. With a sufficiently prolonged exposure at these temperatures in the two-phase region, the W grains dissolve into solution and the composition easily shifts toward the W-rich side 60W-40Ti (at.%) of the miscibility gap in the phase diagram. See Figure 3. During the delay time, cooling of the region below the solidus has begun; nevertheless, the combination of two factors can enhance further shifting past the miscibility gap

29

to the W-rich end 80W-20Ti (at.%) of the phase diagram. These factors are the additional temperature rise during the irreversible work of consolidation in the sample and the presence of the nearby, still relatively hot, TiC. Slow cooling adjacent to the TiC will maintain near-equilibrium conditions that could permit the allowed phase separation beyond the miscibility gap.

The heating of the transition region is not as rapid; however, the temperature also crosses the solidus. Consequently, prior to consolidation, the solid solution may only reach a hypermonotectoid composition within the miscibility gap, 35W-65Ti (at.%). Again, with the rise in temperature during compaction, some shift to a richer W content could occur. The cooling in this region is generally not rapid enough to completely quench-in this metastable solid solution. However, it is sufficiently slow to allow partial phase separation within short, micron-length distances. In certain areas, when the combination of local heat content and cooling rate permit, the initial hypermonotectoid composition to dissociate (i.e., travel along the opposite sides of the miscibility gap solvus) typical monotectoid structures can result.

Lastly, in the core region, W, heated gradually to the isothermal plateau to a temperature below T_m Ti, dissolves in Ti to form a Ti-rich solid solution of 20W-80Ti (at.%). In spite of the heat added during consolidation, this region is quenched quickly as heat is conducted out directly, unimpeded, into the steel fixture through the densified ZrO_2 thermal insulation and steel anvil inserts.

Samples fabricated using higher and lower n_{TiC}/n_s values contain similar microstructures differing in the location and width of the morphological transition zones. Since the initial heat pulse appears to affect the peak temperatures attained in the fixture only, it may be concluded that all samples in the CSA-HEC fixture, regardless of the n_{TiC}/n_s, undergo similar thermal histories.

3.2.3 Anneal and Hardness Characteristics. Analysis of the annealed samples indicates that with increasing temperatures significant changes can be made to the microstructure of the W-Ti

alloy. Limited by its relatively short duration, the heat treatment mainly resulted in the modification of the Ti-rich matrix, but was insufficient to cause rearrangement and increase dispersion of the W grains.

The types of substructures formed in the annealed samples are similar to those already identified in the untreated samples and consistent with the W-Ti phase diagram. At 700 and 1,000° C, although the characteristics of the Ti-rich matrix are altered, the W grain morphology and overall edge-to-core structure are preserved. Specifically, after treatment at 700° C, the initially homogeneous Ti-rich matrix at the sample's core region is found to be composed of monotectoid structures only. Treatment at 1,000° C results in the formation of grain boundary and in-grain precipitates within the Ti-rich matrix. At 1,400° C, the original alloy structure is lost and replaced entirely by a uniform structure of W grains surrounded by a W-rich solid solution, i.e., like that of the untreated sample's edge region.

The Vickers microhardness of the untreated W-Ti alloys was about 5.0 ± 0.1 GPa. This value is typical of the hardness range of mild steels. As expected, the introduction of the monotectoid structure at 700° C and the fine precipitates at 1,000° C causes the microhardness of the alloy to increase slightly to 5.2 ± 0.2 and 5.3 ± 0.1, respectively. Corresponding to the modification of the sample's microstructure, at 1,400° C there is a modest reduction in microhardness to 4.7 ± 0.2.

3.2.4 Fracture and Interfacial Characteristics. SEM examination of fracture surfaces reveals no significant changes in the dominant failure mode between edge and core regions of the sample. A typical fracture surface from the core region for the sample diagrammed in Figure 11 exemplifying a mixed intergranular and transgranular failure mode is shown in Figure 12. (It may be noted that this surface was produced by simply impact-loading the sample at room temperature.) The majority of grains failing by transgranular fracture tend to be in the proximity of the Ti-rich phase. Grains failing by intergranular fracture, however, are predominantly localized within the W aggregates. In these regions, fine pores trapped between the interstices can also be observed. The separation of failure modes into two distinct zones is a clear

31

indication that satisfactory bonding is limited to those regions where the Ti managed to infiltrate into the W particle aggregates.
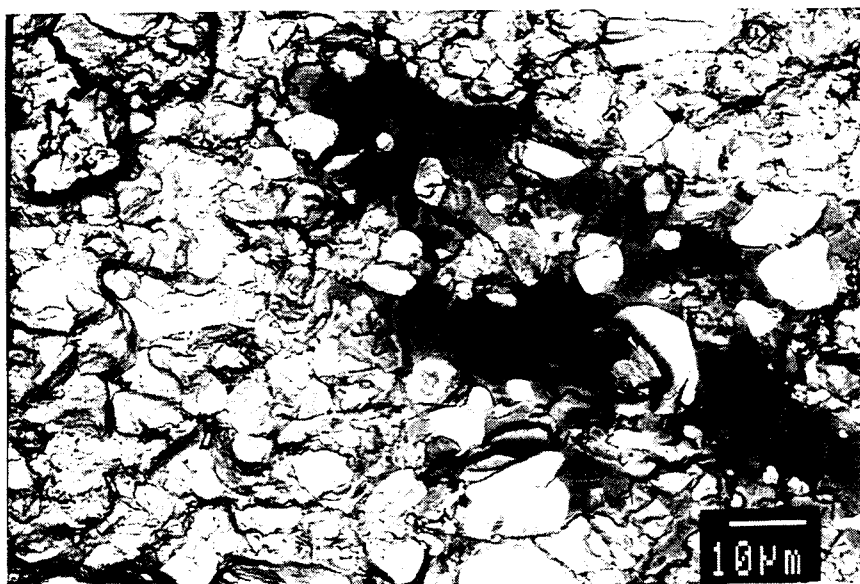
Figure 12. <u>Backscattered electron micrograph of a fracture surface from the core region of the W-Ti sample shown previously in Figure 11.</u>

Although annealing was expected to promote intergranular bonding, neither microhardness measurements nor fracture surfaces from the annealed samples reflect a substantial improvement. In fact, with increasing temperatures, the number of grains failing by intergranular fracture increased.

As evidenced by the nonuniform failure mode of the samples, it was necessary to characterize and evaluate the extent of wetting and solid solution formation near the W grain/Ti-rich matrix interface. Limited by the resolution of the SEM, such details could only be seen effectively with a TEM. Because the regions within the W grain aggregates were impenetrable to the electron

32

beam, TEM observations were restricted to interfaces that were well-developed, i.e., with adequate wetting between the components, usually found near the edge of the Ti matrix. Figure 13 displays a bright field image of a typical area, found in the core region of the sample between two adjacent W particles infiltrated by Ti. In the image, the black areas correspond to the W grains and the gray areas to various solid solution levels between W and Ti. As seen in the figure, the interfacial region is heavily populated by randomly distributed precipitate clusters. A continuous solid solution layer and some of the precipitates can also be noticed adhering to the surface of the W grains. Results of semiquantitative EDS spot analyses, indicated in the image, showed 33W-66Ti (at.%) for area A and 55W-45Ti (at.%) for area B. The presence of the hashed fine structure within the precipitates are indications of a heavily deformed medium. It may be noted that, in observations of interfacial regions, no evidence of particle fragmentation or attrition was found. This is consistent with the rearrangement and deformation stages of dynamic compaction, characteristic of "soft" metals.

Figure 13. Bright field transmission electron micrograph of typical interfacial precipitate substructures found in the W-Ti samples.

33

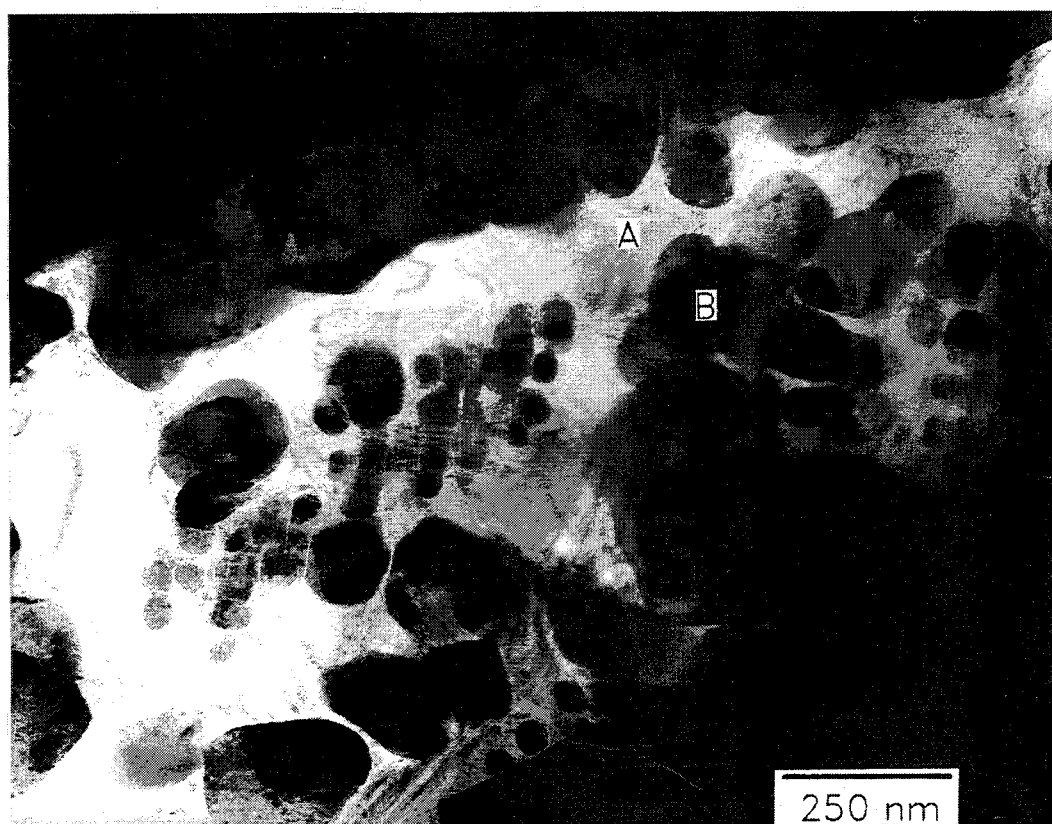As expected, TEM observations of the sample verified that the structural nonuniformity extends to the W/Ti interface, indicative of an extremely high-rate, nonequilibrium process. It is most likely that in the absence of long diffusion times, due to the rapid heating during the SHS phase, compounded by the structural defects introduced during consolidation and the rapid cooling in the CSA-HEC fixture thereafter, the formation of a compositionally uniform W grain/Ti matrix interface is prevented. Instead, in the presence of the conditions elaborated previously, a weaker, less desirable nonuniform structure develops.

Based on the observed microstructures of both untreated and high-temperature, heat-treated samples, it may be concluded that modification and refinement of the existing Ti-rich matrix can be facilitated with relative ease. Because of the limitations imposed by the phase relationship between W and Ti, the desired dissociation of the Ti-rich matrix into its components is more likely accomplished at lower temperatures, e.g., 500° C, well below the monotectoid temperature. With decreased diffusion rates, perhaps longer soaking times, and reduced cooling rates, the dissociation, as well as the homogenization of the Ti-rich matrix could be enhanced.

4. CONCLUSIONS

It has been demonstrated that full density W-Ti alloy disks can be fabricated with a new Combustion Synthesis Assisted HEC technique. Specifically, a W+Ti powder bed is preheated by the heat release of a Ti+C combustion synthesis reaction, and, when the bed is isothermal, it is consolidated by the detonation of an explosive. The inner core of the disk formed by this method is relatively free of cracks and consists of W particle agglomerates surrounded by a partially continuous Ti-rich matrix. Fracture surfaces of the samples reveal a mixed mode of inter and transgranular fracture, indicative of a brittle yet moderately well-bonded sample. TEM observations of the regions surrounding the W grains show that the CSA-HEC process produces a highly heterogeneous interface with precipitate and similar nonequilibrium substructures.

Several key factors have been identified in the CSA-HEC process. For successful consolidation, the c/m must be adjusted to reduce shock-induced damage without compromising

34

the sample density. Similarly, the value of the n_{TiC}/n_s must be large enough such that the sample is isothermal at one time in the heating cycle, yet, at the same time, the temperature at the inner core should not exceed significantly the melting point of the Ti component. In spite of limitations imposed on the sample's microstructure by the rapid heating/cooling cycle in the CSA-HEC system, further improvements could be facilitated using finer Ti precursor. The use of finer Ti may result in a reduction of the W contiguity and hence an increase in W particle dispersion. Ultimately, an ideal system would comprise the consolidation of uniformly dispersed Ti in W, i.e., W particle precursors coated with a thin layer of Ti. Finally, the CSA-HEC samples could be easily subjected to a low-temperature post-consolidation annealing treatment to remove temperature and shock-induced nonuniformities and residual stresses as well as homogenize the Ti-rich matrix and W/Ti interface.

INTENTIONALLY LEFT BLANK.

6. REFERENCES

1. Askeland, D. R. <u>The Science and Engineering of Materials.</u> Boston, MA: PWS-Kent Publishing Company, 2d ed., 1989.

2. Olofson, C. T., G. E. Meyer, and A. L. Hoffmanner. "Processing and Applications of Depleted Uranium Alloy Products." MCIC-76-28, Battelle Laboratories, Metals and Ceramics Information Center, Columbus, OH, September 1976.

3. Eckelmeyer, K. H. "Diffusional Transformations, Strengthening Mechanisms, and Mechanical Properties of Uranium Alloys." <u>Metallurgical Technology of Uranium and Uranium Alloys,</u> vol. 1, Physical Metallurgy of Uranium and Uranium Alloys, American Society for Metals, Metals Park, OH, pp. 129–200, 1982.

4. Rabin, B. H., A. Bose, and R. M. German. "Characteristics of Liquid Phase Sintered Tungsten Heavy Alloys." <u>International Journal Powder Metall.</u>, vol. 25, no. 1, pp. 21–27, January 1989.

5. Magness, L. S., and T. G. Farrand. "Deformation Behavior and Its Relationship to the Penetration Performance of High-Density KE Penetrator Materials." <u>Proceedings of the 1990 Army Science Conference,</u> Durham, NC, pp. 149–164, May 1990.

6. Rogers, H. C. "Adiabatic Shearing - General Nature and Material Aspects." <u>Segamore Army Materials Research Conference Proceedings.</u> Material Behavior Under High Stress and Ultra High Loading Rate. Edited by J. Mescall and V. Weiss, New York: Plenum Press, pp. 110–118, 1983.

7. Staker, M. R. "The Relation Between Adiabatic Shear Instability Strain and Material Properties." <u>Acta. Met.</u>, vol. 29, no. 4, pp. 683–689, April 1981.

8. Stelly, M., and R. Dormeval. "Adiabatic Shearing." <u>Metallurgical Applications of Shock-Wave and High-Strain-Rate Phenomenon.</u> Edited by L. E. Murr, K. P. Staudhammer, and M. A. Meyers, New York: Plenum Press, pp. 607–632, 1986.

9. Murr, L. E., K. P. Staudhammer, and M. A. Meyers (eds). <u>Metallurgical Applications of Shock Wave and High-Strain-Rate Phenomena.</u> New York: Marcel Dekker, Inc., 1986.

10. Massalski, T. B., H. Okamoto, P. R. Subramanian, L. Kacprzak, and William W. Scott (eds.). <u>Binary Alloy Phase Diagrams.</u> New York: 2d ed., 1990.

11. Murray, J. L. The (Ti-W) Titanium-Tungsten System, Bull. Alloy Phase Diag., vol. 2, no. 2, pp. 192–196, September 1981.

12. Goetzel, C. G. Treatise on Powder Metallurgy: Vol. I, Technology of Metal Powders and Their Products. New York: Interscience Publisher's, Inc., 1949.

13. Goetzel, C. G. Treatise on Powder Metallurgy: Vol. II, Applied and Physical Powder Metallurgy. New York: Interscience Publishers, Inc., 1949.

14. Bradbury, S. (ed.). Source Book on Powder Metallurgy. American Society for Metals, Metals Park, OH, 1979.

15. Kuczynski, G. C. Sintering Processes, New York: Plenum Press, 1980.

16. Smith, D. W. "Elements of Powder Metallurgy." Powder Metallurgy, Applications, Advances, and Limitations. Edited by E. Klar. American Society for Metals, Metals Park, OH, 1983.

17. German, R. M. Liquid Phase Sintering. New York: Plenum Press, 1985.

18. Toshihito, K., and R. M. German. "Processing Effects on the Mechanical Properties of Tungsten Heavy Alloys." International Journal Refract. Hard Met., vol. 9, no. 1, pp. 40–45, March 1990.

19. Bourguignon, L. L., and R. M. German. "Sintering Temperature Effects on a Tungsten Heavy Alloy." International Journal Powder Metall., vol. 24, no. 2, pp. 115–121, April 1988.

20. Kang, T. K., E. T. Henig, and G. Petzow. "Influence of Heat Treatment on the Mechanical Properties of 90W-7Ni-3Fe Heavy Alloys." Z. Metallkd., vol. 78, no. 4, pp. 250–258, April 1987.

21. Bose, A., and R. M. German. "Sintering Atmosphere Effects on Tensile Properties of Heavy Alloys." Metall. Trans. A., vol. 19A, no. 12, pp. 2467–2476, October 1988.

22. Bose, A., B. H. Rabin, and R. M. German. "Liquid Phase Sintering of Tungsten Heavy Alloys in Vacuum." Met. Powder Rep., vol. 42, no. 12, pp. 834–839, December 1987.

23. Farooq, S., P. B. Kemp, R. M. German, and A. Bose. "Effect of Initial Oxygen Content and Sintering Atmosphere Dew Point on the Properties of Tungsten Based Heavy Alloys." International Journal Refract. Hard Met., vol. 8, no. 4, pp. 236–243, December 1989.

24. Bose, A., D. M. Sims, and R. M. German. "High Strength Tungsten Heavy Alloys with Molybdenum Additions." International Journal Refract. Hard Met., vol. 7, no. 2, pp. 98–102, June 1988.

25. Bose, A., and R. M. German. "Microstructural Refinement of W-Ni-Fe Heavy Alloys by Alloying Additions." Metall. Trans. A, vol. 19A, no. 12, pp. 3100–3103, December 1988.

26. Bose, A., G. Jerman, and R. M. German. "Rhenium Alloying of Tungsten Heavy Alloys." Powder Metall. Int., vol. 21, no. 3, pp. 9–13, June 1989.

27. Bose, A., and R. M. German. "Matrix Composition Effects on the Tensile Properties of Tungsten-Molybdenum Heavy Alloys." Metall. Trans. A, vol. 21A, no. 5, pp. 1325–1327, May 1990.

28. Ramakrishnan, K. N., and G. S. Upadhyaya. "Effect of Compositions and Sintering on the Densification and Microstructure of Tungsten Heavy Alloys Containing Copper and Nickel." J. Mater. Sci. Lett., vol. 9, no. 4, pp. 456–459, April 1990.

29. Kipphut, C. M., A. Bose, S. Farooq, and R. M. German. "Gravity and Configurational Energy Induced Microstructural Changes in Liquid Phase Sintering." Metall. Trans. A, vol. 19A, no. 8, pp. 1905–1913, August 1988.

30. Rabin, B. H., and R. M. German. "Microstructure Effects on Tensile Properties of Tungsten-Nickel-Iron Composites." Metall. Trans. A, vol. 19A, no. 6, pp. 1523–1532, June 1988.

31. Chung, J. G., and D. J. Duquette. "Stress Corrosion Cracking Behavior of Tungsten Heavy Alloys in Sodium Chloride Solution." Corrosion Science, vol. 44, no. 7, pp. 435–442, July 1988.

32. Posthill, J. B., and D. V. Edmonds. "Matrix and Interfacial Precipitation in the W-Ni-Fe System." Metall. Trans. A, vol. 17A, no. 11, pp. 1921–1934, November 1986.

33. Magness, L. S. Private Communication. U.S. Army Research Laboratory, Aberdeen Proving Ground, MD.

34. Gourdin, W. H. "Dynamic Consolidation of Metal Powders." Prog. Mat. Sci., vol. 30., no. 1, pp. 39–80, January 1986.

35. O'Donnell, R. G. "Rapid Compaction of Materials - A Review." Mat. Forum, vol. 10, no. 3, pp. 163–176, March 1987.

36. Thadhani, N. N. "Shock Compression Processing of Powders." Adv. Mater. and Manuf. Proc., no. 4, pp. 493–549, April 1988.

37. James, P. J. "Fundamental Aspects of the Consolidation of Powders." Powder Met. Int., vol. 4, no. 2, pp. 82–85, no. 3, pp. 145–149, no. 4, pp. 193–198, 1972.

38. Clyens, S., and W. Johnson. "The Dynamic Compaction of Powdered Materials." Mat. Sci. and Eng., vol. 30, pp. 121–139, 1977.

39. Rumpf, H. <u>Agglomeration</u>. Edited by W. A. Knepper. New York: Interscience, New York, p. 379, 1962.

40. Rohde, R. W. "Equation of State of Shock-Loaded Tungsten at 950° C." <u>J. of Appl. Phys.</u>, vol. 40, no. 7, pp. 2988–2993, June 1969.

41. Boade, R. R. "Dynamic Compression of Porous Tungsten." <u>J. of Appl. Phys.</u>, vol. 40, no. 9, pp. 3781–3785, August 1969.

42. O'Donnell, R. G. "Explosive Consolidation of Tungsten Powder." <u>Proceedings of the 1987 Australian Conference on Materials for Industrial Development</u>, University of Canterbury, Christchurch, New Zealand, 24–26 August 1987.

43. Roman, O. V., and V. G. Gorobtsov. "Fundamentals of Explosive Compaction of Powders." <u>Shock Waves and High-Strain-Rate Phenomena in Metals: Concepts and Applications</u>. Edited by M. A. Meyers and L. E. Murr. New York: Plenum Press, pp. 829–841, 1981.

44. Gourdin, W. H. "Energy Deposition and Microstructural Modification in Dynamically Consolidated Metal Powders." <u>J. Appl. Phys.</u>, vol. 55, no. 1, pp. 172–181, January 1984.

45. Linse, V. D. "Dynamic Compaction of Metal and Ceramic Powders." <u>Proceedings of the Sagamore Army Material Research Conference on Innovation in Materials Processing</u>, vol. 30, New York: Plenum Press, pp. 381–404, 1985.

46. Cross, A. "Try Hot Explosive-Compacting for Sintered Powder Products." <u>Iron Age</u>, vol. 184, no. 26, pp. 48–50, December 1959.

47. Gorobtsov, V. G., and O. V. Roman. "Hot Explosive Pressing of Powders." <u>International Journal Powder Metall. and Powder Tech.</u>, vol. 11, no. 1, pp. 55–60, January 1975.

48. Marley, W. F. "Powder Metallurgy Developments in the Soviet Union." <u>International Journal Powder Metall. and Powder Tech.</u>, vol. 13, no. 1, pp. 55–60, 1977.

49. Thompson, E. R. "High Temperature Aerospace Materials Prepared by Powder Metallurgy." <u>Annual Rev. Mater. Sci.</u>, vol. 12, pp. 213–242, 1982.

50. Bhalla, A. K. "Hot Explosive Compaction of Metal Powders." <u>Trans. Powder Metal. Assoc. India</u>, vol. 7, no. 9, pp. 1–8, September 1980.

51. Birla, N. C., and W. Krishnaswamy. "Consolidation of Prealloyed Ti-6Al-2Sn-4Zr-2Mo Spherical Powders." <u>Powder Met.</u>, vol. 24, no. 4, pp. 203–209, 1981.

52. Wang, S. L., M. A. Meyers, and A. Szeket. "Warm Shock Consolidation of IN 718 Powder." <u>J. Mater. Sci.</u>, vol. 23, no. 5, pp. 1786–1804, May 1988.

53. Ferreira, A., M. A. Meyers, N. N. Thadhani, S. N. Chang, and J. R. Kough. "Dynamic Compaction of Titanium Aluminides by Explosively Generated Shock Waves: Experimental and Materials Systems." Metall. Trans. A, vol. 22A, no. 3, pp. 685–695, March 1991.

54. Shang, S. S., K. Hokamoto, and M. A. Meyers. "Hot Dynamic Consolidation of Hard Ceramics." J. Mater. Sci., vol. 27, no. 20, pp. 5470–5476, October 1992.

55. Raybould, D., D. G. Morris, and G. A. Cooper. "A New Powder Metallurgy Method." J. Mater. Sci., vol. 14, no. 10, pp. 2523–2526, October 1979.

56. Taniguchi, T., and K. Kondo. "Hot Shock Compaction of Alpha-Alumina Powder." Adv. Ceram. Mat., vol. 3, no. 4, pp. 399–402, April 1988.

57. Yoshida, M., Y. Yoshioka, Y. Kimura, H. Hirabayashi, A. B. Sawaoka, and R. A. Puemmer. "Explosive Hot Consolidation of Alumina Powder. Influence on Structure." Aerospace, Refractory and Advanced Materials Advances in Powder Metallurgy, vol. 6, pp. 199–209, Metal Powder Industries Federation, Princeton, NJ, 1991.

58. Kecskes, L. J. Unpublished Work.

59. Rhinehart, J. S., and J. Pearson. Explosive Working of Metals. New York: MacMillan Company, 1963.

60. Gabriel, K. A., S. G. Wax, and J. W. McCauley (eds). Materials Processing by Self-Propagating High-Temperature Synthesis (SHS). DARPA/ARMY SHS Symposium Proceedings, MTL-SP-87-3, Daytona Beach, FL, 21–23 October 1985.

61. Munir, Z. A. "Synthesis of High-Temperature Materials by Self-Propagating Combustion Methods." Cer. Bull., vol. 67, no. 2, pp. 342–349, February 1988.

62. Munir, Z. A., and J. B. Holt (eds). Combustion and Plasma Synthesis of High-Temperature Materials. New York: VCH Publishers, Inc., 1990.

63. Niiler, A., L. J. Kecskes, T. Kottke, P. H. Netherwood, Jr., and R. F. Benck. "Explosive Consolidation of Combustion Synthesized Ceramics: TiC and TiB2." BRL-TR-2951, U.S. Army Ballistic Research Laboratory, Aberdeen Proving Ground, MD, December 1988.

INTENTIONALLY LEFT BLANK.

APPENDIX A:

REVIEW OF PRIOR HEC EFFORTS

INTENTIONALLY LEFT BLANK.

In their article, Gorobtsov and Roman defined the basic issues associated with the hot explosive consolidation (HEC) process and provided some data on the compaction of Ni and Ti powders.[1] The design calls for a simple and safe system to heat containers of powders near explosives, their transfer to the explosive charge, and the necessary remote control system for placing the charge onto the hot powder container surface. Additionally, the container that will prevent the oxidation of the powders during heating, pressing, and cooling, and steps to avoid thermal detonation of the explosive were also described. The experimental design, shown in Figure A-1, consisted of a base plate, sealed container with powder, guidance system, thermal insulation, explosive charge, plane wave generator, and a distance control system for setting off the explosive charge. The powder sample was first placed in a seamless container that was hermetically sealed and welded. The initial density of the powder was approximately 50% T.D. The sealed container was heated for 30 min in a nearby electric furnace at temperatures of $800°$ C and $1,000°$ C for Ti (T_m Ti $= 1,670°$ C) and $800°$ C and $1,100°$ C for Ni (T_m Ni $= 1,450°$ C). While the powders were being heated in the furnace, the explosive driver system (explosive and plane wave generator) and base plate were mounted and assembled. After the detonator was armed, the furnace was opened and the hot powder container pushed along the guidance system to locate it beneath the explosive charge. The elapsed time between the transfer from the furnace to the detonation of the explosive was less than 20 s. Fairly large, 10-mm × 100-mm × 180-mm flat plates were consolidated with the technique.

Gorobtsov and Roman claimed full density for both Ni and Ti when the powders were heated prior to compaction. Tensile and Charpy impact strength tests of the HEC samples showed high ductility and toughness. These results implied that the HEC compacts were strong enough for machining and mechanical working such as rolling and forging without a prior need for sintering. While samples compacted at room temperature revealed a preferential deformation in the direction of the shock-wave front, the HEC samples showed an equiaxed grain structure typical of primary recrystallized metals. With higher heating temperatures, larger nonuniform grain sizes were obtained that were more characteristic of secondary recrystallization. It was concluded that

---

[1]Gorobtsov, V. G., and O. V. Roman. "Hot Explosive Pressing of Powders." International Journal Powder Metall. and Powder Tech., vol. 11, no. 1, pp. 55–60, January 1975.

Figure A-1. Schematic diagram of the hot explosive pressing setup used by Gorobtsov and Roman for nickel and titanium powders. From Gorobtsov and Roman (1975).[1] 1 - base plate, 2 - sealed container with powder, 3 - guidance system, 4 - thermoisolation, 5 - main explosive charge, 6 - plane wave generator, 7 - distance control system for setting off the explosive charge.

[1]Gorobtsov, V. G., and O. V. Roman. "Hot Explosive Pressing of Powders." International Journal Powder Metall. and Powder Tech., vol. 11, no. 1, pp. 55-60, January 1975.
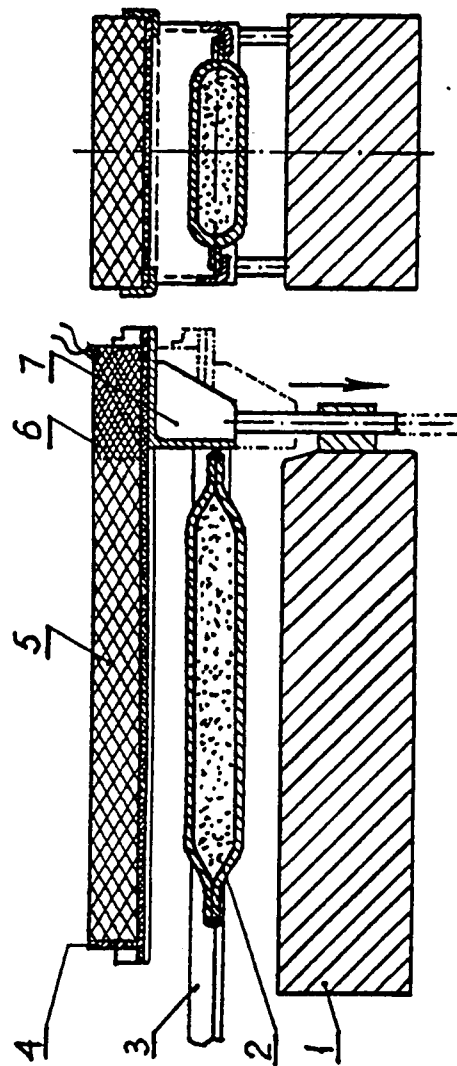
HEC above the recrystallization temperature of the material would result in full density compacts. The authors speculated that in the course of extensive plastic deformation, the underlying mechanism responsible for this structure is that of dynamic recrystallization caused by the joint action of high pressures and high temperatures.

HEC has also been addressed by Bhalla in India.[2] Not much different in its approach and findings, this effort mainly attempted to establish a broader database of the HEC process. Instead of the planar compaction used in the Soviet work, Bhalla used a cylindrical compaction configuration (Figure A-2). In this system, the precursor powder mixture was placed in a sealed tube, preheated in a furnace, quickly removed, transferred, and dropped into the compaction fixture, and subsequently consolidated to full density.

The effect of explosive compaction energy, heating temperatures, and heating times were evaluated for a variety of metal powders. In the compaction of Ni, Ti, Fe, Cu, and Al, it was clearly demonstrated that HEC, above the recrystallization temperature, was solely governed by the impact energy input, and, temperature and time had little influence on sample density. In the case of Ti, compaction in the beta phase region gave higher densities than compaction in the alpha phase region. With Ni, it was found that the shape of the precursor, whether it was spherical or irregular, had no pronounced effect on the ability to compact the metal to full density. Because of the high temperature malleability and plasticity of the powders, the energy requirements (amount of explosive) of HEC were found to be substantially lower than explosive compaction performed at room temperature. Bhalla, much like the Soviets, found that the compacts produced with HEC have superior mechanical properties and require no additional sintering.

In another comparative study, Birla, using Bhalla's HEC design, has applied the HEC process to Rotating Electrode Process (REP) Ti-6Al-2Sn-4Zr-2Mo powder.[3] REP powders are usually

---

[2]Bhalla, A. K. "Hot Explosive Compaction of Metal Powders." Trans. Powder Metal. Assoc. India, vol. 7, no. 9, pp. 1–8, September 1980.

[3]Birla, N. C., and W. Krishnaswamy. "Consolidation of Prealloyed Ti-6Al-2Sn-4Zr-2Mo Spherical Powders." Powder Met., vol. 24, no. 4, pp. 203–209, 1981.

spherical in shape with a cast dendritic microstructure. Three impact energies (950 kJ/m^2, 2310 kJ/m^2, and 3880 kJ/m^2) and three temperatures (1223° K, 1273° K, and 1373° K) were used. Again, compaction primarily depended on temperature and the impact energy delivered by the explosive charge. It was shown that an increase in temperature from 1273° K to 1373° K, at the low impact energy compactions, resulted in an increase of the density from 80% T.D. to 95% T.D. However, samples compacted at the highest impact energy were near, or at full density, and the increase in density with a corresponding increase in temperature was negligible. Thus, apparently the compaction was more sensitive to changes in impact energy than to changes in heating temperatures. The samples compacted to full density yielded mechanical properties that were equivalent or better than wrought properties.
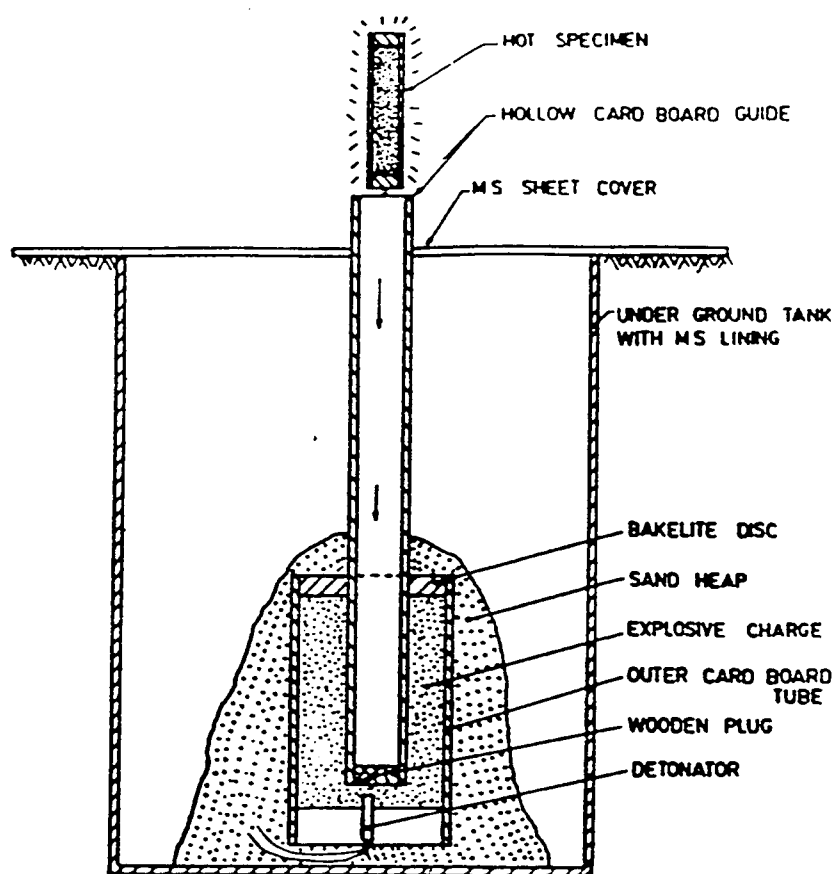

Figure A-2. Bhalla's arrangement for HEC of metal powders.[2]

[2]Bhalla, A. K. "Hot Explosive Compaction of Metal Powders." Trans. Powder Metal. Assoc. India, vol. 7, no. 9, pp. 1–8, September 1980.

More recently, two groups led by Meyers at The New Mexico Institute of Mining and Technology (NMIMT), has warm consolidated REP Inconel 718 and Rapidly Solidified Rate (RSR) titanium aluminide intermetallics.[4,5] Meyers' design used a coaxial double-tube cylindrical configuration and successfully reduced problems associated with previously encountered low consolidation quality, i.e., amount of melt fraction formed, poor intergrain bonding, and cracking. Shock pressure, detonation velocity, and amount of explosive were found to be critical for consolidation. For Inconel 718, preheating to temperatures of 500–750° C appeared to enhance consolidation quality by increasing the amount of intergranular melt fraction. In the case of the brittle titanium aluminides, however, caused by difficulties in eliminating cracking, the effect of preheating (as high as 900° C) was not so clearly understood.

In these studies, Meyers gave descriptions of the experimental procedures, and correlated microstructural features to those of the compaction parameters. The double-tube design is shown in Figure A-3. The sample, in a sealed tube, was removed from an oven and placed on a holder above the explosive setup. When the release solenoid was activated, the sample dropped into its cavity, and the explosive was detonated. The temperature of the sample at compaction was inferred from prior cooling calibrations done on the sealed sample tube. As shown in Figure A-4, in the work with titanium aluminides, for safety reasons, the direction of detonation was inverted, and the sample loading was redesigned.

At NMIMT, Meyers has also worked out the details for a planar compaction geometry to consolidate small samples of diamond and cubic boron nitride (c-BN) ceramics.[6] As shown in Figure A-5, a steel fixture, designed to hold multiple sample capsules, was fitted with an external heating unit. Shock induced damage was reduced by positioning capsules off high symmetry

[4]Wang, S. L., M. A. Meyers, and A. Szeket. "Warm Shock Consolidation of IN 718 Powder." J. Mater. Sci., vol. 23, no. 5, pp. 1786–1804, May 1988.

[5]Ferreira, A., M. A. Meyers, N. N. Thadhani, S. N. Chang, and J. R. Kough. "Dynamic Compaction of Titanium Aluminides by Explosively Generated Shock Waves: Experimental and Materials Systems." Metall. Trans. A, vol. 22A, no. 3, pp. 685–695, March 1991.

[6]Shang, S. S., K. Hokamoto, and M. A. Meyers. "Hot Dynamic Consolidation of Hard Ceramics." J. Mater. Sci., vol. 27, no. 20, pp. 5470–5476, October 1992.

axes and attaching a momentum trap to the base of the fixture. Once the heating element heated the entire steel fixture to the desired temperature, the explosive container could be allowed to slide onto the steel fixture, and remotely detonated. While the uniqueness of this scheme was that up to 12 samples could be synthesized at once, compaction to full density would be limited by inherent mechanical constraints imposed by the capsules. Results of compactions of different size initial powders and their various admixtures with graphite, silicon, and Ti+C at the temperatures of 600° C and 700° C were compared. The use of Ti+C to improve BN properties was inconclusive as the shock wave failed to initiate the Ti+C chemical reaction. The samples compacted at the higher temperature had reduced cracking, improved bonding, and increased hardness. With increasing grain size, cracking increased. In overall quality, samples of c-BN fared better than those of diamond.

In addition to the use of explosives, the idea of powder consolidation by a light gas gun arrangement has been first carried out by Raybould and others.[7,8] These efforts were claimed by the authors to be less dangerous and easier to control than explosive compaction. Preheating the sample prior to consolidation has been carried out by Taniguchi in the consolidation of alpha-Al_2O_3 powder[8]. A schematic diagram is shown in Figure A-6. The compaction of the alumina powder resulted in only moderate density (94–97% T.D.) samples. Densification of fine powders (0.5 μm) occurred by rearrangement and plastic deformation, whereas densification of coarse powders (200 μm) occurred by fracture and fragmentation. As expected, higher shock energies and samples with coarse powder particles suffered more internal cracking than those with finer powder particles. The effect of the heating temperature was mainly noticed in the increase of crystallite size. It was concluded that to produce superior products, fracturing and/or grain growth must be avoided. Consequently, the use of fine powders, lower shock energies, and higher temperatures were recommended. It may be mentioned that due to the arrangement of the heating elements, final removal and extraction of the sample from the compaction die assembly was nontrivial.

---

[7]Raybould, D., D. G. Morris, and G. A. Cooper. "A New Powder Metallurgy Method." J. Mater. Sci., vol. 14, no. 10, pp. 2523–2526, October 1979.

[8]Taniguchi, T., and K. Kondo. "Hot Shock Compaction of Alpha-Alumina Powder." Adv. Ceram. Mat., vol. 3, no. 4, pp. 399–402, April 1988.
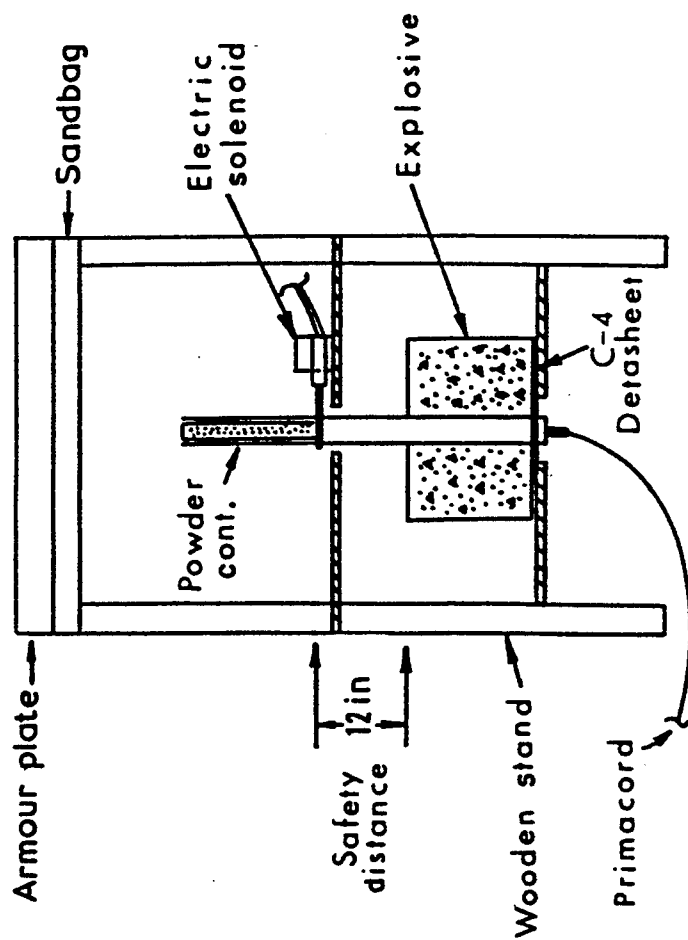
Figure A-3. Wang's arrangement for warm shock consolidation of REP Inconel 718 metal powders.
12 in = 305 mm.[4]

[4]Wang, S. L., M. A. Meyers, and A. Szeket. "Warm Shock Consolidation of IN 718 Powder." J. Mater. Sci., vol. 23, no. 5, pp. 1786–1804, May 1988.

A
- Detonator
- PVC Tube
- Explosive
- Flyer Tube
- Upper Solenoid
- Counterweight
- Sample Capsule
- Wood Frame
- Guide Tube
- Push Tube
- Lower Solenoid

B
- Detonator
- PVC Tube
- Explosive
- Flyer Tube
- Sample Capsule
- Upper Solenoid
- Push Tube
- Wood Frame
- Guide Tube
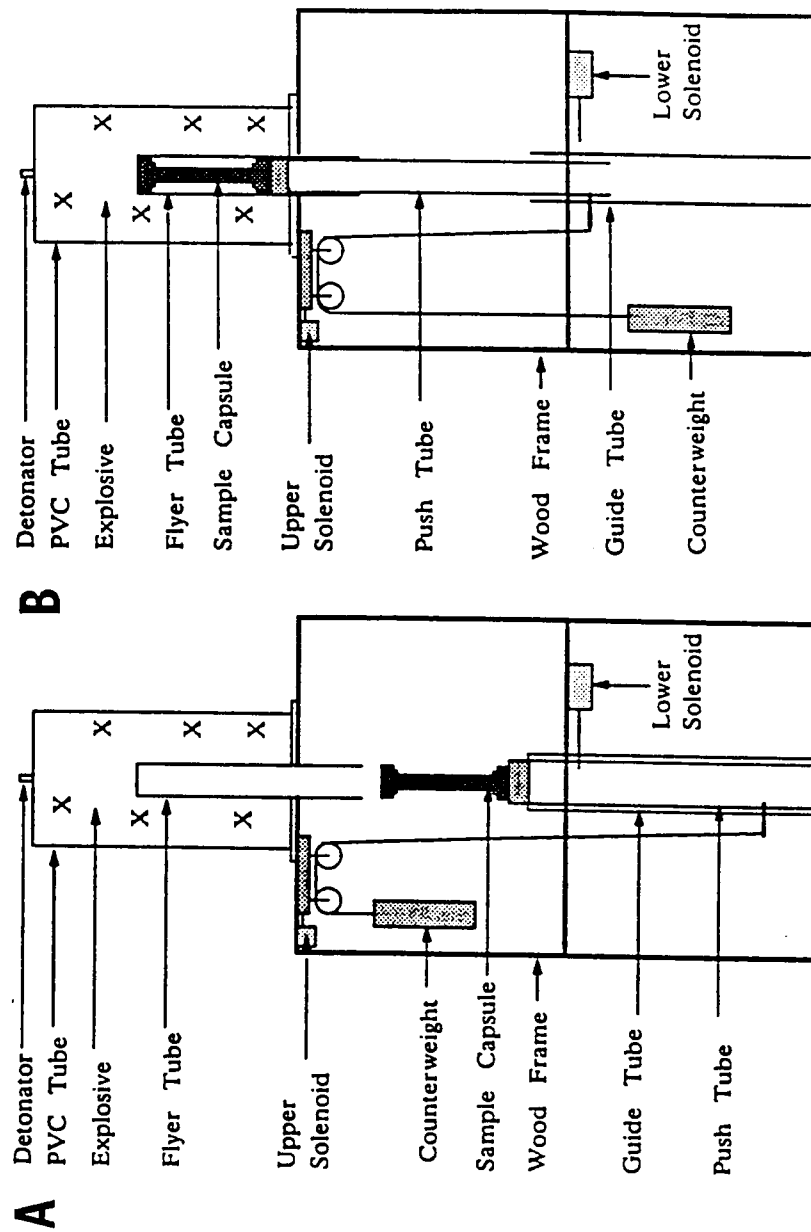- Counterweight
- Lower Solenoid

Figure A-4. Ferreira'a arrangement for warm shock consolidation of titanium aluminide intermetallic powders showing capsule in initial position is 17A and in final position in 17B.[5]

[5]Ferreira, A., M. A. Meyers, N. N. Thadhani, S. N. Chang, and J. R. Kough. "Dynamic Compaction of Titanium Aluminides by Explosively Generated Shock Waves: Experimental and Materials Systems." Metall. Trans. A, vol. 22A, no. 3, pp. 685–695, March 1991.
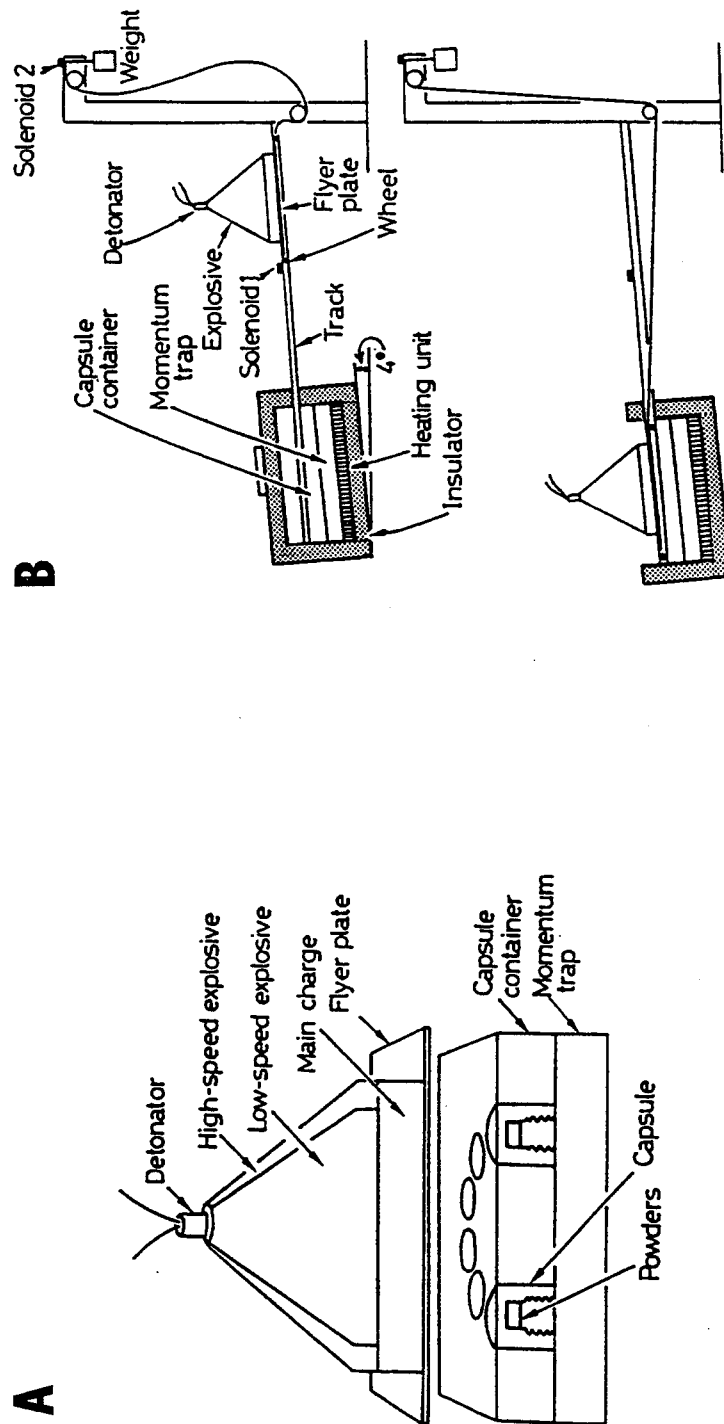
Figure A-5. Shang's arrangement for hot dynamic consolidation of diamond and cubic boron nitride powders showing the planar impact system in 18A and the hot consolidation apparatus in 18B.[6]

[6]Shang, S. S., K. Hokamoto, and M. A. Meyers. "Hot Dynamic Consolidation of Hard Ceramics." J. Mater. Sci., vol. 27, no. 20, pp. 5470–5476, October 1992.
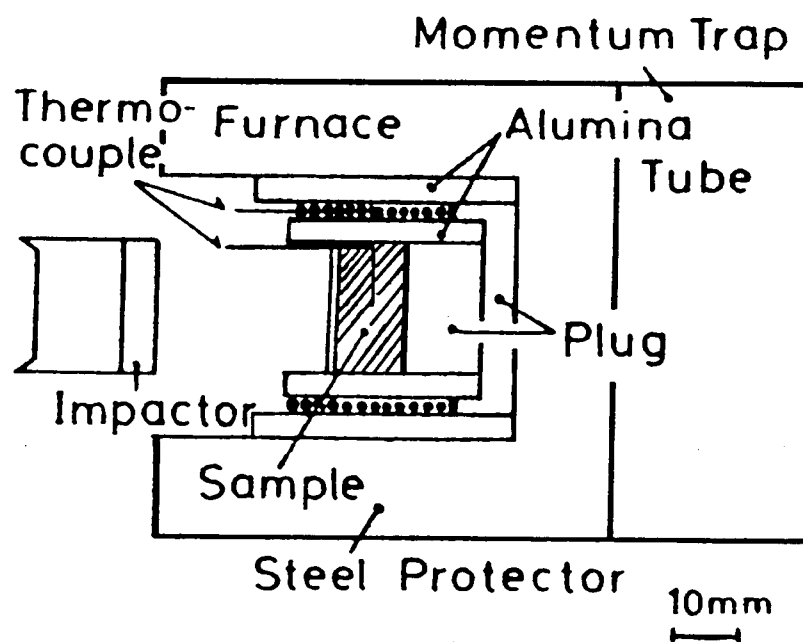
Figure A-6. Schematic diagram showing experimental assembly for hot shock compaction of alpha-alumina powders with a light gas gun.[7]

[7]Taniguchi, T., and K. Kondo. "Hot Shock Compaction of Alpha-Alumina Powder." Adv. Ceram. Mat., vol. 3, no. 4, pp. 399–402, April 1988.

APPENDIX B:

W-Ti ALLOY MOLECULAR WEIGHTS AND DENSITIES

INTENTIONALLY LEFT BLANK.

W-Ti Alloy Molecular Weights And Densities

Tungsten		Titanium		W-Ti	
wt.	at.	wt.	at.	m.w.	density (g/cm^3)
0.000	0.000	1.000	1.000	47.8800	4.5070
0.100	0.028	0.900	0.972	51.7039	4.8808
0.200	0.061	0.800	0.939	56.1915	5.3223
0.300	0.100	0.700	0.900	61.5322	5.8515
0.400	0.148	0.600	0.852	67.9948	6.4977
0.500	0.207	0.500	0.793	75.9741	7.3042
0.550	0.241	0.450	0.759	80.7098	7.7875
0.600	0.281	0.400	0.719	86.0752	8.3394
0.650	0.326	0.350	0.674	92.2047	8.9754
0.700	0.378	0.300	0.622	99.2741	9.7164
0.710	0.389	0.290	0.611	100.8201	9.8795
0.720	0.401	0.280	0.599	102.4151	10.0482
0.730	0.413	0.270	0.587	104.0612	10.2228
0.740	0.426	0.260	0.574	105.7612	10.4035
0.750	0.439	0.250	0.561	107.5176	10.5907
0.760	0.452	0.240	0.548	109.3334	10.7848
0.770	0.466	0.230	0.534	111.2115	10.9862
0.780	0.480	0.220	0.520	113.1553	11.1952
0.790	0.495	0.210	0.505	115.1683	11.4123
0.800	0.510	0.200	0.490	117.2541	11.6380
0.810	0.526	0.190	0.474	119.4170	11.8728
0.820	0.543	0.180	0.457	121.6611	12.1173
0.830	0.560	0.170	0.440	123.9911	12.3721
0.840	0.578	0.160	0.422	126.4122	12.6378
0.850	0.596	0.150	0.404	128.9297	12.9152
0.860	0.615	0.140	0.385	131.5495	13.2050
0.870	0.635	0.130	0.365	134.2779	13.5081
0.880	0.656	0.120	0.344	137.1220	13.8255
0.890	0.678	0.110	0.322	140.0891	14.1582
0.900	0.701	0.100	0.299	143.1875	14.5072
0.910	0.725	0.090	0.275	146.4260	14.8739
0.920	0.750	0.080	0.250	149.8145	15.2596
0.930	0.776	0.070	0.224	153.3634	15.6659
0.940	0.803	0.060	0.197	157.0846	16.0943
0.950	0.832	0.050	0.168	160.9908	16.5469
0.960	0.862	0.040	0.138	165.0963	17.0257
0.970	0.894	0.030	0.106	169.4167	17.5330
0.980	0.927	0.020	0.073	173.9692	18.0714
0.990	0.963	0.010	0.037	178.7732	18.6440
1.000	1.000	0.000	0.000	183.8500	19.2540

INTENTIONALLY LEFT BLANK.

NO. OF COPIES	ORGANIZATION
2	ADMINISTRATOR DTIC ATTN DTIC DDA CAMERON STATION ALEXANDRIA VA 22304-6145
1	CDR USAMC ATTN AMCAM 5001 EISENHOWER AVE ALEXANDRIA VA 22333-0001
1	DIR USARL ATTN AMSRL OP SD TA RECORDS MGMT 2800 POWDER MILL RD ADELPHI MD 20783-1145
3	DIR USARL ATTN AMSRL OP SD TL TECH LIB 2800 POWDER MILL RD ADELPHI MD 20783-1145
1	DIR USARL ATTN AMSRL OP SD TP TECH PUBS BR 2800 POWDER MILL RD ADELPHI MD 20783-1145
2	CDR US ARMY ARDEC ATTN SMCAR TDC PICATINNY ARSNL NJ 07806-5000
1	DIR BENET LABS ATTN SMCAR CCB TL WATERVLIET NY 12189-4050
1	DIR USA ADVANCED SYSTEMS R&A OFC ATTN AMSAT R NR MS 219 1 AMES RESEARCH CENTER MOFFETT FIELD CA 94035-1000
1	CDR US ARMY MICOM ATTN AMSMI RD CS R DOC REDSTONE ARSNL AL 35898-5010
1	CDR US ARMY TACOM ATTN AMSTA JSK ARMOR ENG BR WARREN MI 48397-5000

NO. OF COPIES	ORGANIZATION
1	DIR USA TRADOC ANALYSIS CMD ATTN ATRC WSR WSMR NM 88002-5502
1	CMDT US ARMY INFANTRY SCHOOL ATTN ATSH CD SECURITY MGR FORT BENNING GA 31905-5660

ABERDEEN PROVING GROUND

NO. OF COPIES	ORGANIZATION
2	DIR USAMSAA ATTN AMXSY D AMXSY MP H COHEN
1	CDR USATECOM ATTN AMSTE TC
1	DIR USAERDEC ATTN SCBRD RT
1	CDR USACBDCOM ATTN AMSCB CII
1	DIR USARL ATTN AMSRL SL I
5	DIR USARL ATTN AMSRL OP AP L

NO. OF COPIES	ORGANIZATION

1	NEW MEXICO INST OF
	  MINING AND TECH
	DEPT OF METALLURGICAL
	  AND MATERIALS ENGR
	ATTN DR O INAL
	SOCORRO NM 87801

1	OSRAM SYLVANIA INC CHEM AND METALLURGICAL DIV ATTN DR J MULLENDORE HAWES ST TOWANDA PA 18848
1	TELEDYNE FIRTH STERLING ATTN DR S CALDWELL 1 TELEDYNE PLACE LAVERGNE TN 37086
1	ULTRAMET INC ATTN DR J STIGLICH 12173 MONTAGUE ST PACOIMA CA 91331
1	UNIV OF CA COLLEGE OF ENGR ATTN DR Z MUNIR DAVIS CA 95616
1	UNIV OF CA SAN DIEGO DEPT OF APPLIED MECHS AND ENGR SCIENCE ATTN DR M MEYERS LA JOLLA CA 92093
2	UNIV OF DELAWARE DEPT OF MECH ENGR ATTN DR I HALL DR J MEAKIN NEWARK DE 19716
1	UNIV OF DELAWARE DEPT OF CHEM ENGR ATTN DR J SCHULTZ NEWARK DE 19716

NO. OF COPIES	ORGANIZATION
	<u>ABERDEEN PROVING GROUND</u>

35	DIR USARL
	ATTN AMSRL SL BS
	    J MORRISSEY
	  AMSRL WT
	    D ECCLESHALL
	    G KLEM
	  AMSRL WT W C MURPHY
	  AMSRL WT WA H ROGERS
	  AMSRL WT WB W D'AMICO
	  AMSRL WT WC J ROCCHIO
	  AMSRL WT WD
	    D DANIEL
	    A GAUSS JR
	    C HOLLANDSWORTH
	    L KECSKES (3 CPS)
	    P BERNING
	    A NIILER
	    F PIERCE
	    G THOMSON
	  AMSRL WT WE J TEMPERLEY
	  AMSRL WT TA
	    R BENCK
	    W BRUCHEY
	    W GILLICH
	    W GOOCH
	    G HAUVER
	    T HAVEL
	    E HORWATH
	    D MACKENZIE
	    P NETHERWOOD JR
	  AMSRL WT TC
	    W DE ROSSET
	    E KENNEDY
	    W LEONARD
	    L MAGNESS
	  AMSRL WT TD
	    A DIETRICH JR
	    T FARRAND
	    K FRANK
	    P KINGMAN

NO. OF
COPIES ORGANIZATION

1   . GOVT INDUSTRIAL RSCH
        INST
      ATTN DR N SATA
      4 5 1 NIGATAKE
      MIYAGINO KU
      SENDAI MIYAGI 983 JAPAN

1   NAT RSCH INST FOR METALS
      ATTN DR Y KAIEDA
      2 3 12 NAKAMEGURO
      MEGURO KU
      TOKYO 153 JAPAN

1   OSAKA UNIV
      ATTN DR Y MIYAMOTO
      IBARAKI
      OSAKA 567 JAPAN

1   RYUKOKU UNIV
      ATTN DR M KOIZUMI
      1 5 YOKOYA
      OE CHO
      OTSU SHIGA 520 21 JAPAN

2   TOKYO INST OF TECH
      ATTN DR A SAWAOKA
            DR O ODAWARA
      4259 NAGATSUATA
      MIDORI KU
      YOKOHAMA 227 JAPAN

USER EVALUATION SHEET/CHANGE OF ADDRESS

This Laboratory undertakes a continuing effort to improve the quality of the reports it publishes. Your comments/answers to the items/questions below will aid us in our efforts.

1. ARL Report Number _____ARL–TR–669_____ Date of Report ___January 1995___

2. Date Report Received _____

3. Does this report satisfy a need? (Comment on purpose, related project, or other area of interest for which the report will be used.) _____

_____

_____

4. Specifically, how is the report being used? (Information source, design data, procedure, source of ideas, etc.)_____

_____

_____

5. Has the information in this report led to any quantitative savings as far as man-hours or dollars saved, operating costs avoided, or efficiencies achieved, etc? If so, please elaborate. _____

_____

_____

6. General Comments. What do you think should be changed to improve future reports? (Indicate changes to organization, technical content, format, etc.) _____

_____

_____

_____

CURRENT
ADDRESS

Organization _____

Name _____

Street or P.O. Box No. _____

City, State, Zip Code _____

7. If indicating a Change of Address or Address Correction, please provide the Current or Correct address above and the Old or Incorrect address below.
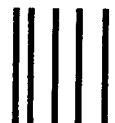
OLD
ADDRESS

Organization _____

Name _____

Street or P.O. Box No. _____

City, State, Zip Code _____

(Remove this sheet, fold as indicated, tape closed, and mail.)
(DO NOT STAPLE)

DEPARTMENT OF THE ARMY

OFFICIAL BUSINESS

BUSINESS REPLY MAIL
FIRST CLASS PERMIT NO 0001, APG, MD

Postage will be paid by addressee

**Director
U.S. Army Research Laboratory
ATTN: AMSRL-OP-AP-L
Aberdeen Proving Ground, MD 21005-5066**